



ASTRO-H Space X-ray Observatory White Paper

Accreting Pulsars, Magnetars, & Related Sources

S. Kitamoto (Rikkyo University), T. Enoto (RIKEN & NASA/GSFC),
 S. Safi-Harb (University of Manitoba), K. Pottschmidt (UMBC & NASA/GSFC),
 C. Ferrigno (University de Geneve), M. Chernyakova (Dublin Institute for Advanced Studies),
 T. Hayashi (JAXA), N. Hell (LLNL¹), K. Kaneko (Tokyo University of Science), D. Khangulyan (JAXA),
 T. Kohmura (Tokyo University of Science), H. Krimm (NASA/GSFC), K. Makishima (University of Tokyo),
 T. Nakano (University of Tokyo), H. Odaka (JAXA), M. Ohno (Hiroshima University),
 M. Sasano (University of Tokyo), S. Sugita (Ehime University), Y. Terada (Saitama University),
 T. Yasuda (Saitama University), and T. Yuasa (JAXA)
 on behalf of the ASTRO-H Science Working Group

Abstract

As the endpoints of massive star evolution, neutron stars are enigmatic celestial objects characterized by extremely dense and exotic nuclear matter, magnetospheres with positrons (antimatter), rapid rotation and ultra-strong magnetic fields. Such an extreme environment has provided an accessible astrophysical laboratory to study physics under conditions unattainable on Earth and to tackle a range of fundamental questions related to: the aftermath of stellar evolution and the powerful explosions of massive stars, the equation of state and physics of some of the most exotic and magnetic stars in the Universe, the workings of the most powerful particle accelerators in our Galaxy and beyond, and the sources of gravitational waves that are yet to be detected. Recent observations revealed a great diversity of neutron stars, including ultra-strongly magnetized pulsars, referred to as “magnetars”, and unusual types of accreting X-ray pulsars. In this white paper, we highlight the prospects of the upcoming X-ray mission, *ASTRO-H*, in studying these highly magnetized neutron stars.

¹Also at Remeis Observatory, FAU.

Complete list of the ASTRO-H Science Working Group

Tadayuki Takahashi^a, Kazuhisa Mitsuda^a, Richard Kelley^b, Felix Aharonian^c, Hiroki Akamatsu^d, Fumie Akimoto^e, Steve Allen^f, Naohisa Anabuki^g, Lorella Angelini^b, Keith Arnaud^b, Marc Audardⁱ, Hisamitsu Awaki^j, Aya Bamba^k, Marshall Bautz^l, Roger Blandford^f, Laura Brenneman^b, Greg Brown^m, Edward Cackettⁿ, Maria Chernyakova^c, Meng Chiao^b, Paolo Coppi^o, Elisa Costantini^d, Jelle de Plaa^d, Jan-Willem den Herder^d, Chris Done^p, Tadayasu Dotani^a, Ken Ebisawa^a, Megan Eckart^b, Teruaki Enoto^q, Yuichiro Ezoe^r, Andrew Fabianⁿ, Carlo Ferrignoⁱ, Adam Foster^s, Ryuichi Fujimoto^l, Yasushi Fukazawa^u, Stefan Funk^f, Akihiro Furuzawa^e, Massimiliano Galeazzi^v, Luigi Gallo^w, Poshak Gandhi^p, Matteo Guainazzi^x, Yoshito Haba^y, Kenji Hamaguchi^h, Isamu Hatsukade^z, Takayuki Hayashi^a, Katsuhiro Hayashi^a, Kiyoshi Hayashida^g, Junko Hiraga^{aa}, Ann Hornschemeier^b, Akio Hoshino^{ab}, John Hughes^{ac}, Una Hwang^{ad}, Ryo Iizuka^a, Yoshiyuki Inoue^a, Hajime Inoue^a, Kazunori Ishibashi^e, Manabu Ishida^a, Kumi Ishikawa^q, Yoshitaka Ishisaki^f, Masayuki Ito^{ae}, Naoko Iyomoto^{af}, Jelle Kaastra^d, Timothy Kallman^b, Tuneyoshi Kamae^f, Jun Kataoka^{ag}, Satoru Katsuda^a, Junichiro Katsuta^u, Madoka Kawaharada^a, Nobuyuki Kawai^{ah}, Dmitry Khangulyan^a, Caroline Kilbourne^b, Masashi Kimura^{ai}, Shunji Kitamoto^{ab}, Tetsu Kitayama^{aj}, Takayoshi Kohmura^{ak}, Motohide Kokubun^a, Saori Konami^r, Katsuji Koyama^{al}, Hans Krimm^b, Aya Kubota^{am}, Hideyo Kunieda^e, Stephanie LaMassa^o, Philippe Laurent^{an}, François Lebrun^{an}, Maurice Leutenegger^b, Olivier Limousin^{an}, Michael Loewenstein^b, Knox Long^{ao}, David Lumb^{ap}, Grzegorz Madejski^f, Yoshitomo Maeda^a, Kazuo Makishima^{aa}, Maxim Markevitch^b, Hironori Matsumoto^e, Kyoko Matsushita^{aq}, Dan McCammon^{ar}, Brian McNamara^{as}, Jon Miller^{at}, Eric Miller^l, Shin Mineshige^{au}, Ikuyuki Mitsuishi^e, Takuya Miyazawa^e, Tsunefumi Mizuno^u, Koji Mori^z, Hideyuki Mori^e, Koji Mukai^b, Hiroshi Murakami^{av}, Toshio Murakami^t, Richard Mushotzky^h, Ryo Nagino^g, Takao Nakagawa^a, Hiroshi Nakajima^g, Takeshi Nakamori^{aw}, Shinya Nakashima^a, Kazuhiro Nakazawa^{aa}, Masayoshi Nobukawa^{al}, Hirofumi Noda^q, Masaharu Nomachi^{ax}, Steve O' Dell^{ay}, Hirokazu Odaka^a, Takaya Ohashi^r, Masanori Ohno^u, Takashi Okajima^b, Naomi Ota^{az}, Masanobu Ozaki^a, Frits Paerels^{ba}, Stéphane Paltaniⁱ, Arvind Parmar^x, Robert Petre^b, Ciro Pintoⁿ, Martin Pohlⁱ, F. Scott Porter^b, Katja Pottschmidt^b, Brian Ramsey^{ay}, Rubens Reis^{at}, Christopher Reynolds^h, Claudio Ricci^{au}, Helen Russellⁿ, Samar Safi-Harb^{bb}, Shinya Saito^a, Hiroaki Sameshima^a, Goro Sato^{ag}, Kosuke Sato^{aq}, Rie Sato^a, Makoto Sawada^k, Peter Serlemitsos^b, Hiromi Seta^{bc}, Aurora Simionescu^a, Randall Smith^s, Yang Soong^b, Łukasz Stawarz^a, Yasuharu Sugawara^{bd}, Satoshi Sugita^j, Andrew Szymkowiak^o, Hiroyasu Tajima^e, Hiromitsu Takahashi^u, Hiroaki Takahashi^g, Yoh Takei^a, Toru Tamagawa^q, Takayuki Tamura^a, Keisuke Tamura^e, Takaaki Tanaka^{al}, Yasuo Tanaka^a, Yasuyuki Tanaka^u, Makoto Tashiro^{bc}, Yuzuru Tawara^e, Yukikatsu Terada^{bc}, Yuichi Terashima^j, Francesco Tombesi^b, Hiroshi Tomida^{ai}, Yohko Tsuboi^{bd}, Masahiro Tsujimoto^a, Hiroshi Tsunemi^g, Takeshi Tsuru^{al}, Hiroyuki Uchida^{al}, Yasunobu Uchiyama^{ab}, Hideki Uchiyama^{be}, Yoshihiro Ueda^{au}, Shutaro Ueda^g, Shiro Ueno^{ai}, Shinichiro Uno^{bf}, Meg Urry^o, Eugenio Ursino^v, Cor de Vries^d, Shin Watanabe^a, Norbert Werner^f, Dan Wilkins^w, Shinya Yamada^r, Hiroya Yamaguchi^b, Kazutaka Yamaoka^e, Noriko Yamasaki^a, Makoto Yamauchi^z, Shigeo Yamauchi^{az}, Tahir Yaqoob^b, Yoichi Yatsu^{ah}, Daisuke Yonetoku^t, Atsumasa Yoshida^k, Takayuki Yuasa^q, Irina Zhuravleva^f, Abderahmen Zoghbi^h, and John ZuHone^b

^aInstitute of Space and Astronautical Science (ISAS), Japan Aerospace Exploration Agency (JAXA), Kanagawa 252-5210, Japan

^bNASA/Goddard Space Flight Center, MD 20771, USA

^cAstronomy and Astrophysics Section, Dublin Institute for Advanced Studies, Dublin 2, Ireland

^dSRON Netherlands Institute for Space Research, Utrecht, The Netherlands

^eDepartment of Physics, Nagoya University, Aichi 338-8570, Japan

^fKavli Institute for Particle Astrophysics and Cosmology, Stanford University, CA 94305, USA

^gDepartment of Earth and Space Science, Osaka University, Osaka 560-0043, Japan

^hDepartment of Astronomy, University of Maryland, MD 20742, USA

ⁱUniversité de Genève, Genève 4, Switzerland

^jDepartment of Physics, Ehime University, Ehime 790-8577, Japan

^kDepartment of Physics and Mathematics, Aoyama Gakuin University, Kanagawa 229-8558, Japan

^lKavli Institute for Astrophysics and Space Research, Massachusetts Institute of Technology, MA 02139, USA

^mLawrence Livermore National Laboratory, CA 94550, USA

ⁿInstitute of Astronomy, Cambridge University, CB3 0HA, UK

^oYale Center for Astronomy and Astrophysics, Yale University, CT 06520-8121, USA

^pDepartment of Physics, University of Durham, DH1 3LE, UK

^qRIKEN, Saitama 351-0198, Japan

^rDepartment of Physics, Tokyo Metropolitan University, Tokyo 192-0397, Japan

^sHarvard-Smithsonian Center for Astrophysics, MA 02138, USA

- ^tFaculty of Mathematics and Physics, Kanazawa University, Ishikawa 920-1192, Japan
- ^uDepartment of Physical Science, Hiroshima University, Hiroshima 739-8526, Japan
- ^vPhysics Department, University of Miami, FL 33124, USA
- ^wDepartment of Astronomy and Physics, Saint Mary's University, Nova Scotia B3H 3C3, Canada
- ^xEuropean Space Agency (ESA), European Space Astronomy Centre (ESAC), Madrid, Spain
- ^yDepartment of Physics and Astronomy, Aichi University of Education, Aichi 448-8543, Japan
- ^zDepartment of Applied Physics, University of Miyazaki, Miyazaki 889-2192, Japan
- ^{aa}Department of Physics, University of Tokyo, Tokyo 113-0033, Japan
- ^{ab}Department of Physics, Rikkyo University, Tokyo 171-8501, Japan
- ^{ac}Department of Physics and Astronomy, Rutgers University, NJ 08854-8019, USA
- ^{ad}Department of Physics and Astronomy, Johns Hopkins University, MD 21218, USA
- ^{ae}Faculty of Human Development, Kobe University, Hyogo 657-8501, Japan
- ^{af}Kyushu University, Fukuoka 819-0395, Japan
- ^{ag}Research Institute for Science and Engineering, Waseda University, Tokyo 169-8555, Japan
- ^{ah}Department of Physics, Tokyo Institute of Technology, Tokyo 152-8551, Japan
- ^{ai}Tsukuba Space Center (TKSC), Japan Aerospace Exploration Agency (JAXA), Ibaraki 305-8505, Japan
- ^{aj}Department of Physics, Toho University, Chiba 274-8510, Japan
- ^{ak}Department of Physics, Tokyo University of Science, Chiba 278-8510, Japan
- ^{al}Department of Physics, Kyoto University, Kyoto 606-8502, Japan
- ^{am}Department of Electronic Information Systems, Shibaura Institute of Technology, Saitama 337-8570, Japan
- ^{an}IRFU/Service d'Astrophysique, CEA Saclay, 91191 Gif-sur-Yvette Cedex, France
- ^{ao}Space Telescope Science Institute, MD 21218, USA
- ^{ap}European Space Agency (ESA), European Space Research and Technology Centre (ESTEC), 2200 AG Noordwijk, The Netherlands
- ^{aq}Department of Physics, Tokyo University of Science, Tokyo 162-8601, Japan
- ^{ar}Department of Physics, University of Wisconsin, WI 53706, USA
- ^{as}University of Waterloo, Ontario N2L 3G1, Canada
- ^{at}Department of Astronomy, University of Michigan, MI 48109, USA
- ^{au}Department of Astronomy, Kyoto University, Kyoto 606-8502, Japan
- ^{av}Department of Information Science, Faculty of Liberal Arts, Tohoku Gakuin University, Miyagi 981-3193, Japan
- ^{aw}Department of Physics, Faculty of Science, Yamagata University, Yamagata 990-8560, Japan
- ^{ax}Laboratory of Nuclear Studies, Osaka University, Osaka 560-0043, Japan
- ^{ay}NASA/Marshall Space Flight Center, AL 35812, USA
- ^{az}Department of Physics, Faculty of Science, Nara Women's University, Nara 630-8506, Japan
- ^{ba}Department of Astronomy, Columbia University, NY 10027, USA
- ^{bb}Department of Physics and Astronomy, University of Manitoba, MB R3T 2N2, Canada
- ^{bc}Department of Physics, Saitama University, Saitama 338-8570, Japan
- ^{bd}Department of Physics, Chuo University, Tokyo 112-8551, Japan
- ^{be}Science Education, Faculty of Education, Shizuoka University, Shizuoka 422-8529, Japan
- ^{bf}Faculty of Social and Information Sciences, Nihon Fukushi University, Aichi 475-0012, Japan

Contents

1	Overview: Strongly Magnetized Neutron Stars	5
1.1	Introduction	5
1.2	Accreting Pulsars	6
1.3	Magnetars	7
2	Probes into Accreting Pulsars and their Environment	9
2.1	X-raying the Environment	9
2.1.1	Mapping the Stellar Wind	9
2.1.2	Searching for Signatures of the Alfven Shell	12
2.2	Cyclotron Line Sources	13
2.2.1	Background and Previous Studies	13
2.2.2	Prospects & Strategy	14
2.2.3	Targets & Feasibility	15
2.2.4	Measuring Polarisation during a Giant Outburst	16
2.3	Super-giant Fast X-ray Transients (SFXTs)	17
2.3.1	Background and Previous Studies	17
2.3.2	<i>ASTRO-H</i> perspectives on SFXTs	18
2.4	Gamma-ray Loud Binaries	18
2.4.1	Introduction	18
2.4.2	PSR B1259-63	19
2.4.3	LSI +61 303	20
3	Probes into Magnetars and their Environment	21
3.1	What makes magnetars and how do they evolve? Probing their supernova progenitors, energetics and evolution	21
3.2	Can we find direct evidence of the strong field?	25
3.2.1	On the link between magnetars and the other classes of neutron stars through a direct measurement of the magnetic field	26
3.3	Unified understanding of the magnetar X-ray spectrum?	27
3.4	How the burst activity is related with the nature of magnetars?	29
3.4.1	Unresolved spectral change during the X-ray outburst	30
3.4.2	Magnetar signatures in the short bursts and giant flares	31
4	Appendix	33
4.1	Acronym	33

1 Overview: Strongly Magnetized Neutron Stars

1.1 Introduction

Since their discovery, neutron stars (NSs) have excited a broad range of interests not only in the astrophysical context, but also in terms of fundamental physics: for example, confirmation of the existence of gravitational waves (Taylor & Weisberg, 1982), high-density nuclear matter inside NSs (Lattimer & Prakash, 2007), and high-magnetic field effects around these enigmatic objects (Harding & Lai, 2006). Since NSs are characterized by extreme conditions, such as dense matter, rapid rotation, and high magnetic field, they have proved to be ideal laboratories to test fundamental physics, which cannot be achieved by ground-based experiments. Even 45 years into their discovery, space-based observations are becoming more important in understanding the growing diversity of these enigmatic objects.

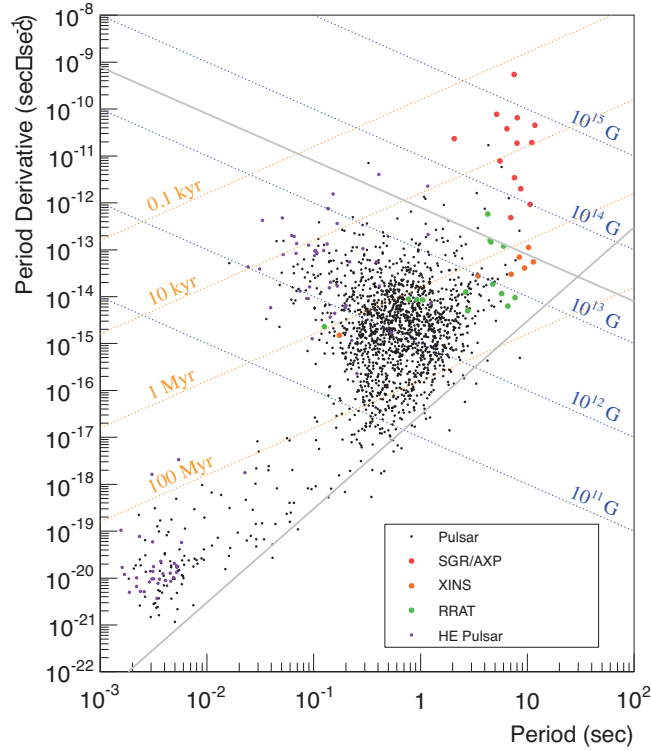


Figure 1: The P - \dot{P} diagram of pulsars shown with lines of constant dipole magnetic field, B , and spin-down age ($\tau_c = \frac{P}{2\dot{P}}$). The black dots show the majority of radio-discovered pulsars believed to be rotation-powered, and the red circles show the X-ray or gamma-ray discovered magnetars addressed in this white paper (see §1.1). Source: ATNF pulsar catalog (Manchester et al., 2005).

Recent multi-wavelength observations from radio to the highest energy gamma-rays have revealed a remarkable diversity of NSs (Kaspi, 2010). Figure 1 shows the distribution of known pulsars based on their measured spin (P) and spin-down (\dot{P}) properties. So far over ~ 1700 pulsars have been discovered in the radio and most of them are thought to be powered by their rotational energy (i.e. Rotation Powered Pulsars; RPPs). Their magnetic field is usually inferred from their spin properties¹, in the 10^{11} – 10^{13} Gauss (1 Tesla = 10^4 Gauss). In addition some accretion-powered pulsars show X-ray “Cyclotron Resonance Scattering Features” allowing us to estimate the magnetic field of the neutron star, see §1.2 and §2.2. On the other hand, Soft Gamma-ray Repeaters (SGRs) and Anomalous X-ray Pulsars (AXPs) have become a rapidly growing new subclass with much higher magnetic fields, $B \sim 10^{14} - 10^{15}$ Gauss and dubbed as “magnetars”. Unlike for rotation-powered or accretion-powered pulsars, the bulk of their X-ray emission appears to be powered by their super-strong magnetic fields. The growing diversity of NSs includes the Rotating Radio Transients (RRATs), X-ray Dim

¹The pulsar’s dipole surface magnetic field is estimated as B_s (Gauss) $\approx 3.2 \times 10^{19} (P/\dot{P})^{1/2}$ where P is in sec.

Isolated NSs (XDINSs), and Central Compact Object (CCOs). Understanding the connection between these classes remains one of the most important questions in this field; multi-wavelength observations continue to provide clues on their nature, emission mechanisms and physical properties. A unified understanding requires a better understanding of their birth environment, evolutionary path, and interaction with their (binary, if applicable) environment.

In this White Paper, we focus on highly magnetized NSs with magnetic fields $B > 10^{12}$ Gauss. These include magnetars (§1.3, §3) as well as accreting pulsars (§1.2, §2). The latter are mostly found in High Mass X-ray Binaries (HMXBs). NS with relatively weaker fields ($B \leq 10^{11}$ Gauss) are usually observed in Low Mass X-ray Binaries (LMXBs), these sources will be reviewed in another White Paper (WP#3, Done, Tsujimoto et al.). There are exceptions, though, like the Low and Intermediate Mass X-ray Binary pulsars GX 1+4 (§2.1.2) and Her X-1 (§2.2). We also include new and not yet fully characterized accreting binary classes like Super-giant Fast X-ray Transients (SFXTs, §2.3) and Gamma-ray Loud Binaries (§2.4) in the current White Paper. Last but not least we also consider peculiar sources that are not necessarily known to harbor a pulsar and can therefore serve as comparison sources (e.g., regarding wind accretion) as well as being unique study objects in their own right, e.g., Cyg X-3 (§2.1.1) or SS 433.

1.2 Accreting Pulsars

Many XRBPs comprise a young neutron star (NS), endowed with a strong B -field ($\sim 10^{12}$ G) and a supergiant or main sequence, “donor” star. The donor star can lose a conspicuous amount of matter through a strong stellar wind and/or via the Roche lobe overflow (see, e.g., Frank et al., 2002). A large part of this material is focused toward the NS as a consequence of the strong gravitational field of this object, and then threaded by its intense magnetic field at several thousand kilometers from the stellar surface. The region in which the ram pressure of the plasma equals the magnetic field pressure is known as the Alfvén surface and in its vicinity all the exchange of angular momentum happens. Once funneled down to the magnetic poles of the NS, accretion columns may form. Here, the gravitational potential energy of the accreting matter is first converted into kinetic energy and then dissipated in the form of X-rays (see, e.g., Pringle & Rees, 1972; Davidson & Ostriker, 1973).

To a first approximation, the B -field lines of the NS rotate rigidly with the surface of the star, and thus the X-ray emission emerging from the accretion column is received by the observer modulated at the spin period of the compact object, if the magnetic and rotational axes are misaligned. Important effects are expected from the interaction of radiation with the strongly magnetized plasma (see below). These effects can be probed on observational grounds studying pulse profiles and time resolved spectra.

As a more important progress expected with the *ASTRO-H*, SXS will probe with high significance the characteristics of the plasma in the stellar wind and its coupling with the Alfvén surface. This is an open field of study, which is receiving further thrust by novel simulations (e.g., Manousakis et al., 2012a) and will receive an observational breakthrough from the high spectral resolution and high effective area of the SXS, which can measure precisely, e.g., the ionization parameter (Tarter et al., 1969). The strong wind, with the velocity of more than 10^8 cm s $^{-1}$, has a strong impact on the emission line profiles. Doppler shift and broadening, coupled with self absorption by the wind itself (Owocki & Cohen, 2001), and P-Cygni profile will be observed (Brandt & Schulz, 2000). The existence of accretion wakes and ionization front of a photo-ionized plasma can be also studied with a modulation of the line profiles induced by the orbital motion. A subject which looks particularly interested is the study of the time variation of iron fluorescence line at the spin period timescale, which might help tracing the ultimate fate of the plasma before being captured by the B -field and unveil the location and extension of the transition zone between the wind and the NS magnetosphere.

The understanding of the broad-band energy spectrum and its time variations can be used to track the X-ray emission pattern close to the NS surface and ultimately constrain the fundamental parameters of a neutron stars, such as its mass, magnetic moment and radius. Among the different radiation processes, the interaction with the magnetic field is probably the most crucial for the XRBPs, as it gives rise to the cyclotron resonant scattering features (CRSFs; see, e.g., Isenberg et al., 1998; Araya-Góchez & Harding, 2000; Schönherr et al., 2007, for recent models). The CRSFs provide a unique tool to directly estimate the magnetic field strength

in the X-ray emitting region close to the NS surface, because the centroid energy of the fundamental appears at $E_{\text{cyc}} = 11.6 B_{12} \times (1+z)^{-1}$ keV. (Here B_{12} is the magnetic field strength in units of 10^{12} G and z is the gravitational redshift in the line-forming region, Wasserman & Shapiro, 1983). If a cyclotron line is detected with high significance in the energy range of the SGD (many are known, see Caballero & Wilms 2012 for a compilation), it can be possible to measure the degree of polarisation, which is induced by the scattering with electrons trapped in a strong magnetic field. This would be a major breakthrough for our understanding of the source emission mechanism, as it would be a very strong constraint on the geometry of the X-ray emitting region, which is currently unknown.

1.3 Magnetars

We expect NSs to acquire their strong magnetic fields up to $\sim 10^{12}$ Gauss or more when their massive progenitors collapse, but the origin of strong magnetism in NSs is one of the biggest unsolved problems in astrophysics. Some of the major challenges for understanding their fundamental properties lie in the difficulties associated with probing observationally their internal structure, the state of nuclear matter, and their magnetic field configuration. Similarly, we know little about how their magnetic fields evolve and whether they decay with time. To tackle these questions, Soft Gamma-ray Repeaters (SGRs) and Anomalous X-ray Pulsars (AXPs), collectively called “magnetars” (Duncan & Thompson, 1992; Thompson & Duncan, 1995), have in the past decade provided an ideal laboratory, particularly in the light of recent multi-wavelength observations and monitoring programs.

Magnetars are a fascinating subclass of NSs (Woods & Thompson, 2006; Mereghetti, 2008) characterized by (i) spin periods in a narrow range of $P \sim 2\text{--}12$ s; (ii) high spin-down rate, \dot{P} , indicative of a young characteristic age $\tau_c \equiv P/2\dot{P} \lesssim 100$ kyr; (iii) dominant emission in X-rays, with luminosity $L_X \sim 10^{34\text{--}36}$ erg s $^{-1}$ which largely exceeds their spin-down luminosity, $\dot{E}_{\text{sd}} = \frac{-2\pi I \dot{P}}{P^3}$ (where I is the pulsar’s moment of inertia); (iv) sporadic X-ray activities on time-scales of msec to years; and (v) no evidence for accretion indicating *isolated* compact objects, unlike the HMXBs. The surface dipole magnetic field of magnetars estimated from P and \dot{P} (see footnote in the Introduction and Figure 1) turns out to be extremely high, $B_s > B_{\text{QED}}$, the so-called quantum electrodynamic critical field of 4.4×10^{13} G at which the Landau level separation exceeds the rest mass energy of an electron, $m_e c^2 = 511$ keV. We note however the recent discovery of lower magnetic field magnetars, discussed later.

Despite the wealth of observational studies dedicated for the study of magnetars, their true nature and their evolutionary link to the other classes of NSs is still not clear. Moreover, the magnetar hypothesis itself remains an open issue. While the magnetar model (Duncan & Thompson, 1992; Thompson & Duncan, 1995) remains the most popular theory for explaining the overall properties of SGRs and AXPs, other models have been proposed and are not yet completely ruled out. These include the fallback disk model (Alpar et al., 2001; Ertan et al., 2009), quark stars model (Ouyed et al., 2006), and white dwarfs model (Malheiro et al., 2012). Therefore, a truly fundamental question related to their intrinsic magnetic fields and the powering mechanism for their observed emission remains to be answered.

One straightforward way of confirming their “magnetar” nature is through a *direct* measurement of their magnetic fields. This can be performed by detecting cyclotron resonance lines as already established in accreting-powered pulsars using the “electron” cyclotron resonance appearing at $E_{\text{ec}} = 11.6 \times (B/10^{12} \text{ G})$ keV; see e.g. (Truemper et al., 1978). Correspondingly, the “proton” cyclotron resonance is expected to appear at an energy

$$E_{\text{pc}} = 0.63 \times (B/10^{14} \text{ G}) \text{ keV}. \quad (1)$$

Although signatures of the proton cyclotron resonance have been reported from only a few magnetars (Ibrahim et al., 2002, 2003; Rea et al., 2003; Gavril et al., 2008a), none of them are considered to be convincing due to the limited energy bands, their transient nature, or insufficient statistics. We are thus urged to search for a much firmer evidence of proton cyclotron resonances using the SXS of *ASTRO-H*. The detailed discussion will be performed in §3.3.

If this subclass indeed exhibits such extreme fields, how do these stars sustain their strong magnetism, and how are the magnetars linked to the canonical NSs with typical $B_s \sim 10^{12}$ G? Since we do not know whether

they are intrinsically different from other ordinary pulsars, an effective approach is to search for transition objects between magnetars and canonical pulsars. Such an object has in fact been discovered and caught in the act of transitioning from a rotation-powered pulsar to a magnetar: the high-magnetic field pulsar J1846–0258 in the supernova remnant Kes 75 (Kumar & Safi-Harb, 2008; Gavril et al., 2008c). Furthermore, more recently, the *Swift* satellite is allowing the detection of sporadic X-ray outbursts, thus increasing the number of magnetars by a few new sources per year. These recent on-going discoveries of the magnetar class implies that this population would be much larger in our Galaxy than we expected before, requiring us to revise our understanding of the formation and evolution both of magnetars and NSs.

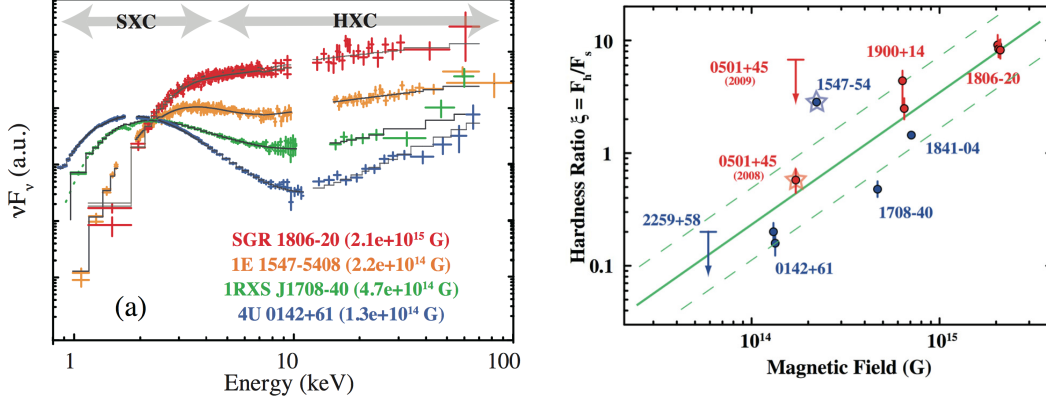


Figure 2: (left) Broadband νF_ν spectra of 4 magnetars observed with *Suzaku* (modified from (Enoto et al., 2010)). To clearly illustrate the difference, each spectrum is normalized at 2 keV. Individual sources are shown in different colors with their magnetic field. (right) Correlation of the broadband HR (=HXC/SXC) to the surface magnetic field.

The discovery of transient magnetars (Ibrahim et al., 2004) and, more recently, the discovery of a low-field (i.e. $B < B_{QED}$) “magnetar” SGR 0418+5729 (Rea et al., 2010) (and a few others, see later) suggest that there is a larger population of magnetar-like objects or “fossil magnetars” in our Galaxy and that the spin-down dipole magnetic field is *not* the only factor determining the magnetar properties. These “fossil” magnetars will be interesting potential targets for *ASTRO-H*. As suggested by such weaker field magnetar activities, the NSs are suggested to store a huge hidden poloidal field component as energy reservoir in addition to the canonical toroidal field component. This is an interesting topic to be related with the supernova explosion mechanism and the formation of magnetars or even the more canonical NSs. In order to observationally address the supernova explosion mechanism, the birth environment and progenitors of magnetars, one promising approach is through X-ray spectroscopy of supernova remnants (SNRs) associated with magnetars. Recent *Chandra* and *XMM-Newton* observations (e.g. Kumar et al. 2012) suggested a high-mass progenitor ($\gtrsim 30 M_\odot$) for an SNR associated with a high-B pulsar; a result that is also supported by multi-wavelength studies of a few magnetars (see e.g. Gaensler et al. 2005; Morton et al. 2007). Related *Suzaku* studies have been also performed for the SNRs Kes 73 and CTB 109 hosting AXP (§3.1).

So far ~ 20 SGRs and AXPs have been discovered in our Galaxy and the Magellanic Clouds. For a long time, they were thought to emit X-rays only below ~ 10 keV. This bright soft X-ray component (hereafter SXC) is represented by a quasi-thermal spectrum with $kT \sim 0.5$ keV hotter than other isolated NSs. A new breakthrough came with *INTEGRAL*’s discovery of an unexpected hard X-ray component (HXC) above ~ 10 keV (Kuiper et al., 2006). This HXC was confirmed by follow-up *Suzaku* observations, covering the SXC and HXC simultaneously thanks to combining the X-ray Imaging Spectrometer (XIS) and the Hard X-ray Detector (HXD) (Enoto et al., 2011). Figure 2 shows νF_ν spectra of four magnetars. The HXC has an extremely hard photon index, $\Gamma_h \sim 1$, almost the hardest among known X-ray sources, and extends up to ~ 100 keV. Although theoretical accounts have not yet been reached (e.g., Thompson & Beloborodov 2005; Baring & Harding 2007), its near-absence in other types of X-ray sources suggests its connection to the strong magnetic fields of magnetars.

It is hence imperative to examine their broad-band spectral properties including both the SXC and the HXC

to understand this enigmatic object. *Suzaku* has performed broad-band (0.8–70 keV) observations of ~ 9 magnetar sources, providing some evidence that two components in the magnetars spectra (i.e. the SXC and HXC described above) systematically change depending on their magnetic field and characteristic age (Enoto et al., 2010). In particular, the HXC becomes weaker relative to the SXC, but harder for older objects. Although SGRs and AXPs first came into astrophysics as unrelated objects, where the former class was discovered through the burst activity while the latter class was recognized as unusually bright X-ray pulsars, the present correlation implies a unification of SGRs and AXPs into one evolutionary path.

Recent exciting discoveries of X-ray outbursts from magnetars also provide us rare opportunities to search for the HXC during active states. Following the *Swift* discoveries of magnetar outbursts, *Suzaku* and *INTEGRAL* follow-up observations successfully detected the enhanced HXC and their gradual decays coinciding with the decay of the SXC: e.g., SGR 0501+4516 (Rea et al., 2009; Enoto et al., 2010c) and 1E 1547.0-5408 (Enoto et al., 2010c; Kuiper et al., 2012; Iwahashi et al., 2013). Although the number of the HXC-confirmed magnetars is gradually increasing, we still don’t know whether all magnetars actually exhibit the HXC in all the states; e.g., the HXC has not yet been confirmed from some persistent emitting sources, such as 1E 2259+586 and 1E 1048.1–5937. In the *ASTRO-H* era, our next step is to investigate the broadband spectra of transient magnetars in their outbursts. In particular, to bring our discoveries during the quiescent states into the next stage, our main strategy will be to perform prompt observations of the HXC just after the onset of the outburst. These questions on a unified understanding of the magnetar evolution will be discussed in detail in §3.2.

Another distinctive feature is sporadic burst activities, short bursts, intermediate flares, and giant flares, usually coinciding with X-ray outbursts. The spectra of SGR bursts detected with *HETE-2* and *Suzaku* were described well by two blackbody components (Olive et al., 2004; Nakagawa et al., 2007). The blackbody temperature can much exceed the normal Eddington limit, probably due to suppression of the Thomson scattering. Thus, the strong magnetic field significantly affects the familiar blackbody radiation. Also, the blackbody radius sometime increases up to 30 km during bursts, suggesting the photosphere to expand to fill the magnetosphere. At the moment, we don’t know why two blackbody components appear. Do they represent the two photo polarizations (O- and X-modes)² which acquire different “photospheres” when $B > B_c$? More fundamentally, is the two-blackbody fit physically meaningful or mimicking a more complex process, e.g., resonant electron cyclotron scattering? In fact, the persistent emission from some magnetars prefer blackbody + power-law modeling to the two-blackbody fit, requiring investigation (§3.5).

2 Probes into Accreting Pulsars and their Environment

2.1 X-raying the Environment

2.1.1 Mapping the Stellar Wind

Many accreting pulsars are part of a High Mass X-ray Binary (HMXB). HMXBs possess a strong stellar wind that can be photoionised by the X-ray emission from the compact object. Hundreds of X-ray emission and absorption lines have been observed with the *Chandra* and *XMM-Newton* gratings for bright wind NS and black hole accretors like **Vela X-1**, **Cen X-3**, **Cyg X-3**, **Cyg X-1**, **4U 1700–37**, or **GX 301–2** (Sako et al., 2002; Schulz et al., 2002; Hanke et al., 2009a; Fürst et al., 2011).

From modelling those lines as well from studying the sometimes extreme flux variability – as, e.g., shown by the supergiant fast X-ray transients (§2.3) or sources like Vela X-1 (Kreykenbohm et al., 2008; Fürst et al., 2010) – it is known that these winds are often structured. They can show focused material streams towards the compact object (Hanke et al., 2009b), can have material trailing the compact object in an accretion wake (Nagase et al., 1992; Manousakis et al., 2012b), and can exhibit instabilities leading to clumping (Feldmeier et al., 2008; Hanke et al., 2009b). In addition several HMXBs are eclipsing sources (e.g., Vela X-1, Cen X-3, 4U 1700–37). Observing the ingress or egress can in principle allow for a detailed look at the atmosphere of the

²Two photon polarizations of which the electric vector is parallel and perpendicular to the magnetic field.

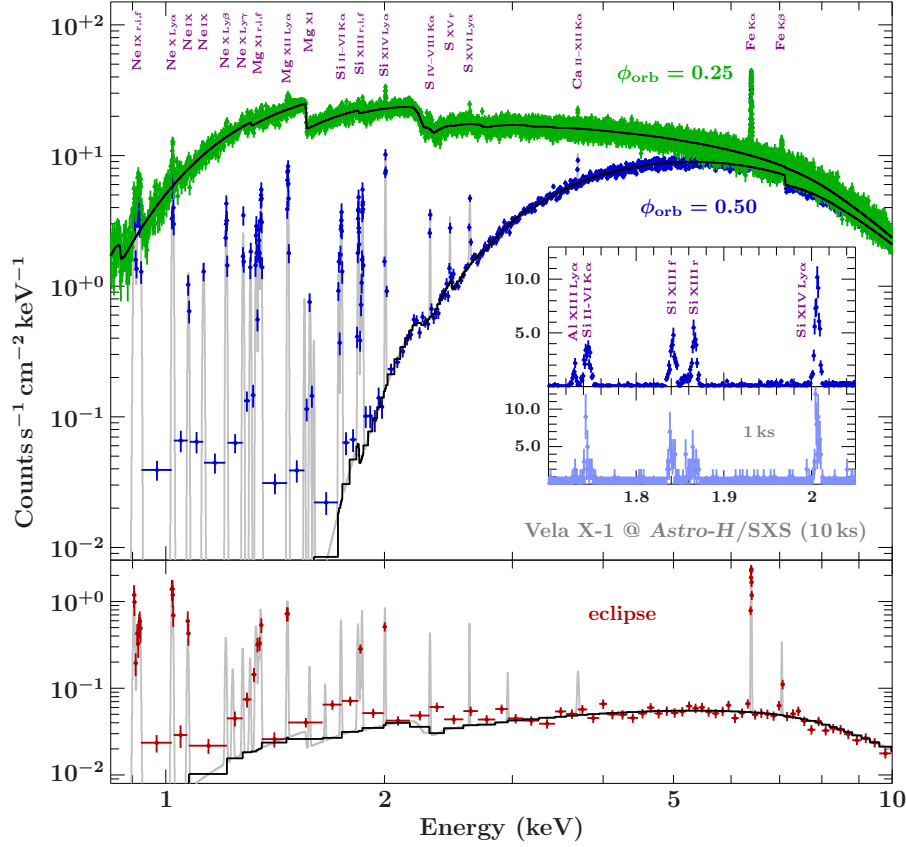


Figure 3: SXS simulations of three 10 ks observations of the accreting pulsar and HMXB Vela X-1 at different orbital phases, based on longer *Chandra* observations (Watanabe et al., 2006). The spectra have been rebinned for clarity, excesses at low energies indicate additional lines. Courtesy M. Kühnel (FAU) and N. Hell (FAU & LLNL).

companion star, e.g., its density and ionisation structure resulting from the interaction with the compact object (Wojdowski et al., 2003; Naik et al., 2011).

Modelling lines and absorption edges from photoionised plasmas, ideally fitting series from the same ion together, has already provided important constraints, e.g., on predominant ionisation stages, ion abundances, and equivalent widths for different sources and orbital phases. However, this is just the beginning of what will be possible using the *ASTRO-H* SXS instrument. Pre-SXS limitations include that wind properties have not yet been spatially resolved. This requires high time resolution line mapping, e.g., through eclipse egress/ingress or of the photoionised accretion wake. The comparatively small effective area of grating spectrometers cannot provide sufficient statistics for such a study, contrary to the SXS, (see below). Such intriguing studies as resolving individual clumps will also become feasible for the first time.

Line spectra of exemplary accreting pulsars — Vela X-1: For a description of system properties see §2.2. Figure 3 shows the SXS view of lines from many highly ionised ions as well as their strong variability over the ~ 9 d orbit. The X-ray continuum spectrum is highly absorbed, especially near phase 0.5 (accretion wake) but the lines still have high equivalent widths, i.e., they are not fully absorbed by this material. SXS observations during the line-rich (near-)eclipse as well as around phase 0.5 can be expected to maximize the scientific return. Figure 4 (egress) and the inset in Figure 3 (wake) show that SXS observations will allow us to determine the evolution of line parameters with unprecedented time resolution of 1-5 ks over a broad energy range. — **Cen X-3:** This system consists of a NS spinning at a period of ~ 4.8 s in an ~ 2.1 d orbit with a O-type supergiant star (see, e.g., references in Suchy et al., 2008). All the phenomena described above – from eclipse to eclipse – could thus potentially be covered by one SXS observation. Near-neutral, He-like, and H-like iron lines have been observed by *Chandra* and *Suzaku* (Iaria et al., 2005; Naik et al., 2011). Outside of eclipse the X-ray

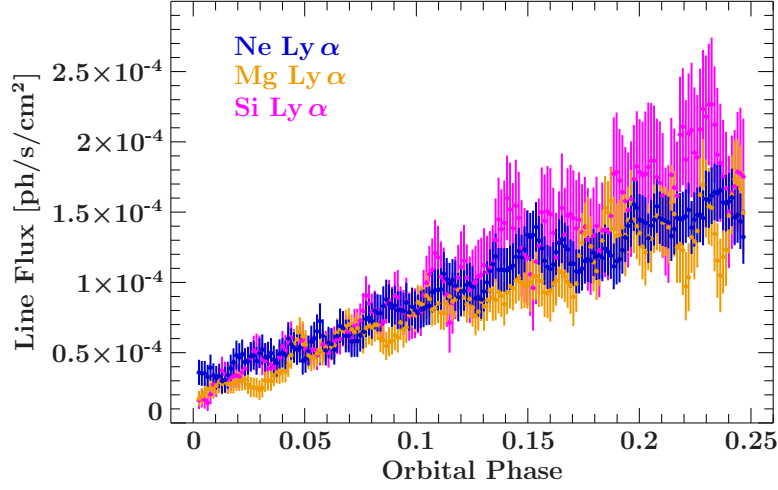


Figure 4: Simulated evolution of the line flux with orbital phase during egress for three prominent lines of Vela X-1. A 5 ks gliding window was applied to 1 ks simulations. The simulated line flux was linearly interpolated between *Chandra* observations at phase 0 and 0.25. The simulated absorbed continuum has been subtracted (N_H was assumed to be modulated with phase according to spherical wind model). The wavy structures are a numerical artifact. Courtesy N. Hell (FAU & LLNL).

spectrum is dominated by sometimes highly variable continuum emission, exhibiting very weak absorption lines mostly from H-like ions (Sako et al., 2002). During eclipse, however, the spectrum is dominated by line emission (Wojdowski et al., 2003). — **GX 301–2:** For a description of system properties see §2.2. That section also presents an SXS simulation of the continuum and line spectrum expected during the bright pre-periastron flare that is a regular feature of the 41.5 d orbital flux variation, see Figure 8. GX 301–2 is characterised by several (near-neutral) fluorescent emission lines, a Compton shoulder of the iron line, and a highly absorbed ionising continuum (Fürst et al., 2011; Watanabe et al., 2003). — **CRSF:** Note that all three of these accreting pulsars are also known cyclotron line (CRSF) sources. Observing their broad band spectra with *ASTRO-H* would thus also allow us to address the scientific objectives described in §2.2.

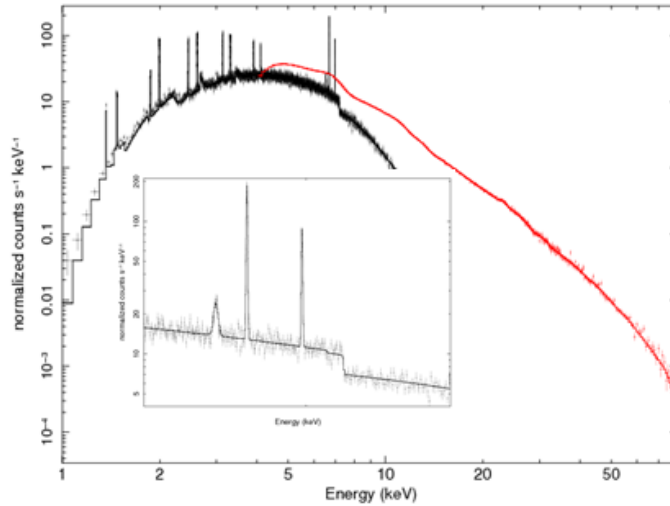


Figure 5: SXS and HXI simulation of a 2 ks observation of Cyg X-3.

A unique wind accreter — Cyg X-3: Located at a distance of 8–10 kpc in the plane of the Galaxy, Cyg X-3

is composed of a compact object in a 4.8 hours orbit with a Wolf-Rayet star. The emission from the system is detected from radio up to GeV energy band. The soft X-rays are thought to arise from the accretion disc, the hard X-rays from the corona, and the radio from the jet (Szostek et al., 2008). This makes interpretation of the data complex and one needs to use timing information along with the spectral one to be able to reconstruct the data in a unique way (Koljonen et al., 2013). Cyg X-3 harbours a large number of emission lines that are especially prominent in the high resolution energy spectra (Paerels et al., 2000). However, due to the low sensitivities of the *RXTE* PCA below 3.5 keV, Koljonen et al. (2013) were able to use only the iron line complex in their analysis. Despite this fact they still have seen dips in the variance spectrum in the energy bins 1.8–1.9 and 2.3–2.4 keV. The dips correspond roughly to the location of some of the strongest emission lines in the X-ray spectra (H-like Si at ~ 2.0 keV and H-like S at ~ 2.5 keV) and could be interpreted as a reduction in variability indicating line production further out from the compact object in the photoionised stellar wind. However, the dips could also be due to the low flux and wide energy bins. Paerels et al. (2000) showed that the iron line complex consists of He-like and H-like iron ions (XXV/XXVI) at 6.7 keV and 6.9 keV, respectively, and cold iron K_{α} at 6.4 keV. However, these lines blend into a single broad feature in the PCA, which makes it difficult to disentangle the two possible emission regions.

Thus a similar exercise done with *ASTRO-H* data will provide a unique chance to study the spectral-timing variability of the source along the orbit using the whole wealth of information coming from spectral lines and using the simultaneous time series for a very broad energy range, which will make it possible to disentangle these different components and see all of them in play simultaneously. The sensitivity of the SXS instrument allows us to get detailed spectra already with a 2 ks exposure (see Figure 5), and thus with a 20 ks observation *ASTRO-H* would be able to trace the spectral variability of the source along the whole orbit.

2.1.2 Searching for Signatures of the Alfven Shell

Fluorescent lines of low ionized iron ions have been observed from some of accretion powered X-ray pulsars. Although its emission region is not well understood, its candidate is an Alfven shell or an inner part of their accretion disk. In these regions, magnetic field and the matter are fiercely competing with each other and information of their dynamical motion of the gas provide us new insights of the environment of accreting neutron stars. The information of the dynamics around the Alfven shell is relating to the strength of the magnetic moment and mass of the neutron stars.

GX 1+4 is not a High Mass X-ray Binary, but is considered to contain a highly magnetized neutron star with $\sim 10^{13}$ G (Makishima et al., 1988). Its prominent K_{α} line has an equivalent width of ~ 200 eV. Its central energy and the 7.1 keV absorption edge indicate the iron ions are almost neutral and suggest its fluorescent origin.

Although *Suzaku* XIS data did not show the energy modulation of the line central energy (< 10 eV), it shows a line broadening with roughly 40–50 eV in standard deviation. These results, the broadening and the small energy modulation, indicate that the line emission region is in a widely extended region of the accretion flow or of the Alfven shell. However, current CCDs, including XIS, have ambiguity of the energy response function for bright point sources due to the SCF-effect (Todoroki et al., 2012). Therefore, SXS, for the first time, makes it possible to study detailed spectroscopy of spin-phase sliced spectra.

The expected Kepler velocity around the Alfven shell is ~ 1000 km s $^{-1}$. Thus the energy shift by this velocity is ~ 200 eV. If the emission lines uniformly come from the Alfven shell, the line width is expected to be $\sim \frac{200}{\sqrt{12}} \sim 60$ eV in standard deviation. By the observation with the SXS, we can expect the detection of a significant broadening and probably a modulation of the width as well as the central energy.

Assuming a 40 ksec observation and analysis of 10 phase sliced spectra, we simulated a 4 ksec observation using best fit parameters obtained by *Suzaku*. An expected spectrum is shown in Figure 6. We assumed a power law continuum with a photon index of 2.9 suffered photo-electric absorption of 4×10^{23} H atoms cm $^{-2}$, and neutral iron fluorescent lines: $K_{\alpha 1}$, $K_{\alpha 2}$, and K_{β} (this line contains several lines but here we represented them by one Gaussian). The intensity-ratio of the three lines is fixed to be 100:50:17 and the line width is fixed to be 10 eV (standard deviation). One sigma error of the line central energy is estimated to be ~ 0.1 eV, which corresponds to 4.7 km sec $^{-1}$. The line width can be also determined with an error of ~ 0.2 eV, which is again

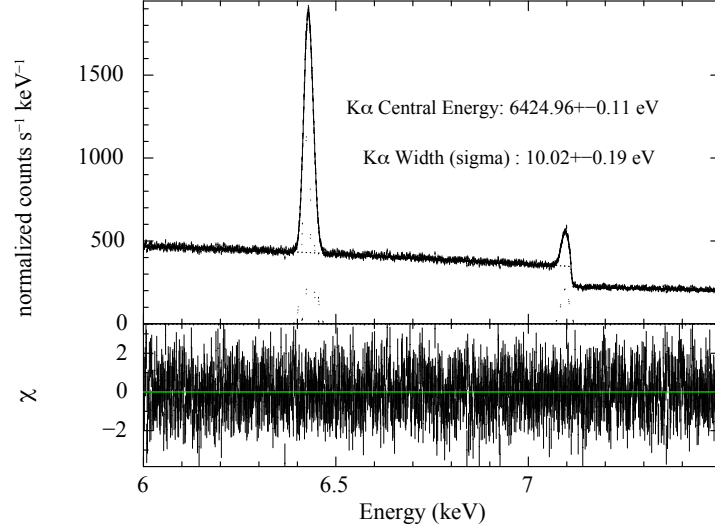


Figure 6: Simulation of the SXS spectrum of GX 1+4. The exposure time is assumed to be 4 ks and the model is an absorbed power law plus three Gaussian lines ($K_{\alpha 1}$, $K_{\alpha 2}$ and K_{β}). The line widths are all assumed to be 10 eV (standard deviation of a Gaussian function).

much less than the expected width. Therefore we can precisely determine an average velocity and velocity dispersion of gas which emits fluorescent lines with only a 1 day observation.

If we can estimate the Kepler velocity at the Alfvén radius from the observed modulation of the central energy, by assuming some accretion flow geometry, we can discuss the relation among mass, magnetic moment of the neutron star and accretion rate. Since the accretion rate can be estimated from the bolometric luminosity, the relation between the mass and the magnetic moment of the neutron star can be deduced.

2.2 Cyclotron Line Sources

2.2.1 Background and Previous Studies

About 25 X-ray binaries show broad absorption-line-like features in their hard X-ray spectrum due to the interaction of the emerging photons with the electrons trapped along the 10^{12} G magnetic field. The energy of these features is the only direct measurement of a magnetic field in the X-ray emitting region ($E \simeq 11.6 \times n \times B_{12}$ keV, where n is the harmonic number and B_{12} is the magnetic field in units of 10^{12} G). The underlying continuum emission is produced by Comptonization of the radiation produced in the optically thick part of the accretion flow or at its footprint on the NS surface and has a smooth power-law shape exponentially attenuated at high energy. Although its phenomenological description is fairly simple, the detailed physics are still a matter of debate (Becker et al., 2012, and references therein), as well as the strong variability at all time scales, which is thought to be due to the clumpy nature of the plasma, when it flows within the magnetosphere. Reproducing on theoretical grounds the observables is still a challenge which would yield informations on basic properties of the neutron star such as the magnetic field configuration and its interaction with the accreted matter.

Timing signatures are of paramount importance to understanding these objects. In particular the “pulse profile”, which is the X-ray emission of the XRBPs folded at the spin period of the NS. Pulse profiles are remarkably stable when averaged over several rotational cycles, reflecting the trapping of plasma along the magnetic field lines. Significant variations in the shape of profiles are observed when the XRBPs undergo transitions between different X-ray luminosity states, such as reported in the cases of EXO 2030+275 and V 0332+65, (Klochkov et al., 2008; Tsygankov et al., 2010, and references therein). At high luminosity, a radiative shock forms in a relatively extended (a few km) accretion column, and the radiation is emitted mainly from its lateral walls in the form of a “fan beam”. At lower luminosities, the radiative shock is suppressed, matter reaches the base of the column with the free-fall velocity and X-rays are emitted nearly vertically in a “pencil beam”. In this state, the height of the column can be significantly reduced, and for very weak sources,

it reduces to a hot-spot on the NS surface. Correspondingly, variations of the centroid energy of the cyclotron scattering features with the luminosity have been observed and tentatively been interpreted as variations of the accretion column height (Staubert et al., 2009; Klochikov et al., 2011, 2012). This picture still needs to be confirmed by further observations.

The majority of XRBPs show significant changes in the spectral energy distribution of the X-ray emission at different pulse phases. This is due to a variety of factors that change during the rotation of the star. In particular, the cross section of the scattering between photons and electrons trapped in a magnetic field strongly depends on the angle between the photon trajectory and the magnetic field lines.

The interplay between the extraordinary and ordinary polarisation modes of photons propagating in a strongly magnetised plasma is expected to produce phase variable linear polarisation at a level as high as 80% in correspondence to the cyclotron scattering features and for particular pulse phases (the polarisation fraction is lower for energies out of resonance, Meszaros et al., 1988). Different imprints are expected to appear in the spin-phase resolved emission for different emission patterns: an anti-correlation between polarisation fraction and X-ray intensity in the case of pencil beam, and anti-correlation in case of a fan beam. The linear polarisation fraction can be lowered of $\sim 30\%$ by relativistic light bending, which causes emission from both magnetic poles to be simultaneously visible. The theoretical predictions are highly uncertain as they depend on the unknown system geometry and emission beaming.

Advances in our understanding of these objects have come from *BeppoSAX* (Boella et al., 1997) and *RXTE* (Bradt et al., 1993) observations, which have however a limited spectral resolution, while the superb performance of *Suzaku* (Mitsuda et al., 2007) is hampered by the spectral gap between the soft and the hard X-rays. *NuSTAR* (Harrison et al., 2013) has provided a quantum leap in the 5–60 keV energy domain spectral analysis, which is comparable to the possible achievements of the HXI.

2.2.2 Prospects & Strategy

ASTRO-H provides a wide spectral coverage, coupled with excellent timing capabilities (the latter for SXS, HXI, and SGD) and unprecedented spectral resolution in the broad energy range relevant for the physics of HMXB (0.1–100 keV). The significant overlap in the bands of the instruments provides a very robust inter calibration tool, which helps in reducing the systematic uncertainties. It is, therefore, an ideal laboratory for studies of objects emitting over a wide energy range combining the excellence of previous missions. The limited effective area with respect to past (e.g., *RXTE*) and current (e.g., *XMM-Newton*) instruments is not an issue for bright X-ray binaries.

Polarisation has not been measurable in X-rays below a few hundreds keV so far. The Soft Gamma-ray Detector (SGD) on board *ASTRO-H* can perform this measurement using the Compton kinematics above ~ 50 keV. This will open an unprecedented observational window, which will provide stringent constraints on the theoretical models when combined with the pulse-phase and luminosity dependent spectral variations of the cyclotron line energy and underlying continuum. This will potentially trim down the enormous parameter space which is currently left almost unconstrained in the theoretical interpretation. In particular, the geometrical configuration of the magnetic field and thus of the emitting regions on the NS is largely unknown as well as the shape of the accretion stream close to the NS surface: matter could fall in a filled or hollow column, or in portions of it (Basko & Sunyaev, 1976). Theoretical models are already challenged by observation, which in turn are still not sufficient to find a solution due to limited spectral resolution or band pass limitations.

The broad band data with high spectral and timing resolution provided by *ASTRO-H* will provide an unprecedented robust benchmark for theory. Many of the sources that display cyclotron lines or are strong candidates are transient, e.g., **4U 0115+63**, **V 0332+53**, **GRO J1008–57**, **GX 304–1**, **EXO 2030+375**, or **A 0535+26**. In the case that one of them shows a giant outburst it will be an excellent target for *ASTRO-H*, providing the best chance of observing polarisation, see §2.2.4. Bright persistent sources that will allow for detailed time-, luminosity-, and pulse-phase-resolved studies of the cyclotron lines and the X-ray continuum, are, e.g., **Vela X-1**, **GX 301–2**, **Cen X-3**, **Her X-1**, or **4U 1626–67**. In the following we present simulations of *ASTRO-H* observations for the persistent cyclotron line sources Vela X-1 and GX 301–2. Vela X-1 is characterised by

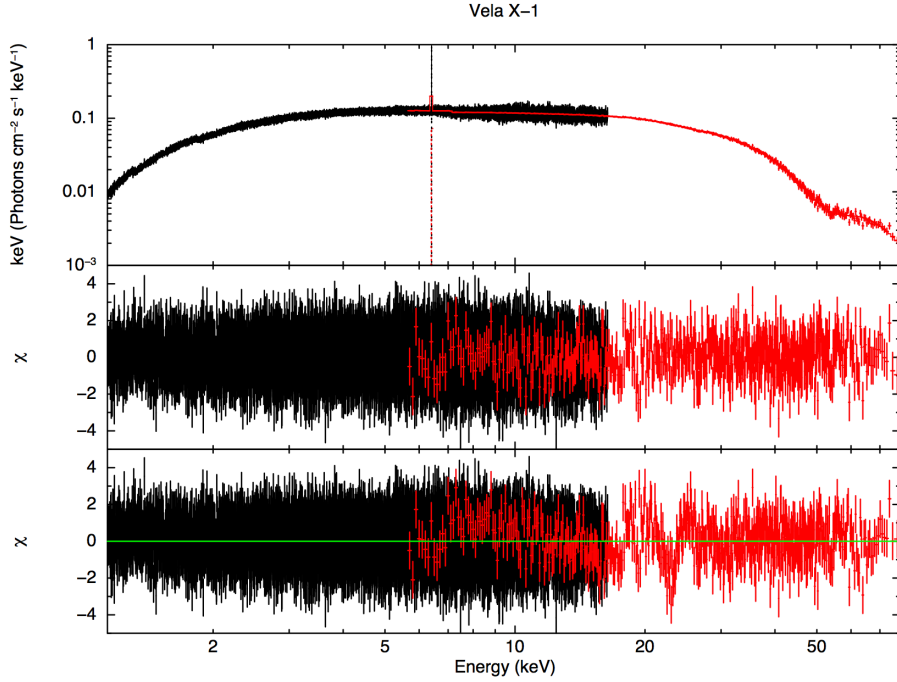


Figure 7: Simulated SXS and HXI spectrum for a 100 ks exposure of Vela X-1 using the continuum model and two CRSFs at ~ 25 keV and ~ 55 keV from Maitra & Paul (2013). Middle panel: Residuals using Lorentzian cyclotron line profiles, as for the simulation. Bottom panel: Residuals from a model with Gaussian optical depths lines, structure is present around the CRSF fundamental at ~ 25 keV.

significant orbital-phase-dependent variability (§2.1.1) as well the irregular occurrence of strong flares and off-states (Fürst et al., 2010). GX 301–2 presents a marked pre-periastron flare and heavy intrinsic absorption in the stellar wind, thought to be due to an accretion stream preceding the NS (Fürst et al., 2011, and references therein). Both sources also show pronounced emission lines due to neutral and ionised material (Figure 3 and Figure 8).

2.2.3 Targets & Feasibility

Vela X-1 (4U 0900–40) is an eclipsing and persistently active system consisting of a massive ($23M_{\odot}$; $34R_{\odot}$) B0.5 1b supergiant and a neutron star. It has an orbital period of 8.964 days and shows only slight eccentricity ($e \sim 0.1$). The neutron star is deeply embedded in the strong stellar wind of the companion; the typical X-ray luminosity is $\sim 4 \times 10^{36}$ erg/s. It exhibits pulsations with a period 283 s. Cyclotron lines appear at ~ 25 and 55 keV (La Barbera et al., 2003; Kreykenbohm et al., 2002). Maitra & Paul (2013) analysed a 100 ks *Suzaku* observation and found an interesting dip-feature linked to enhanced absorption from a partial covering component at a particular pulse phase. This will be better constrained by the SXS. A 100 ks simulation with SXS and HXI shows that *ASTRO-H* will provide an improved determination of the energy and width of the cyclotron scattering features in comparison to existing datasets (Figure 7; see §2.1.1 for a simulation including the emission lines from the stellar wind). With such an observation it would be possible to discriminate between different line profile models for the first time.

Relatively strong polarisation could be present in the SGD band due to the harmonic cyclotron scattering feature at ~ 50 keV. In Vela X-1 the first harmonic is unusually strong. We have verified that in 50 ks, it would be possible to detect a polarisation fraction of 35%.

GX 301–2 consists of an accreting NS with a period of ~ 685 s fed by the surrounding stellar wind of the B type emission line companion Wray 977. Doroshenko et al. (2010) determined an orbital period of 41.482 ± 0.001 days. In the SXS band, GX 301–2 is characterised by several fluorescent emission lines, ris-

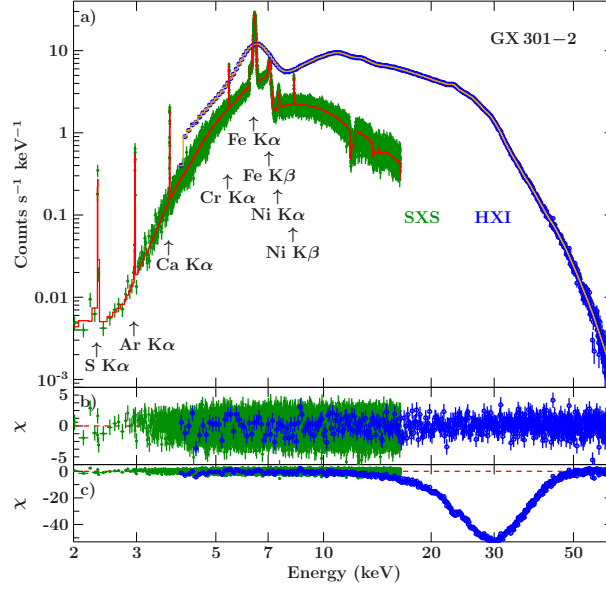


Figure 8: a) Simulated SXS and HXI spectra for a 50 ks exposure on GX 301–2 based on the analyses by Fürst et al. (2011) and Suchy et al. (2012). Emission lines are indicated. b) Residuals from a best fit. c) The residuals from a model with the exclusion of the cyclotron absorption feature at ~ 30 keV. Courtesy M. Kühnel (FAU) and N. Hell (FAU & LLNL).

ing above the highly absorbed ionising continuum (Fürst et al., 2011). A Compton shoulder of the iron line is visible both in the *XMM-Newton* CCD spectrum and in the high-resolution grating spectrum of *Chandra* (Watanabe et al., 2003) and could be studied in detail by the SXS. The cyclotron absorption feature is located at about 30 keV. We have simulated a 50 ks observation based on existing analyses (Figure 8 Fürst et al., 2011; Suchy et al., 2012) and verified that the emission lines are detected by the SXS with high significance, allowing the observer to fully characterise the wind environment, while the HXI is able to constrain the shape of the cyclotron absorption line with high accuracy.

2.2.4 Measuring Polarisation during a Giant Outburst

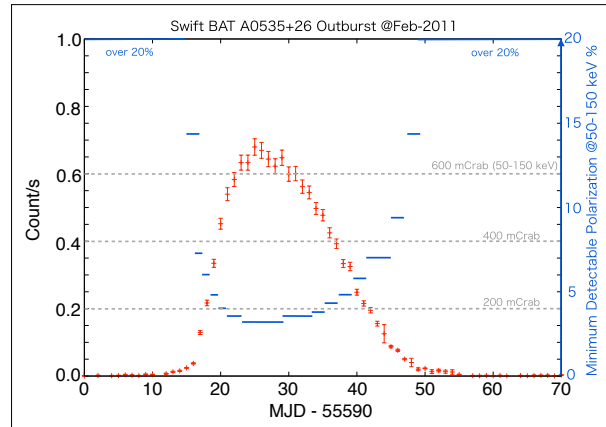


Figure 9: Measurable polarisation fraction of the X-ray signal in the 50–100 keV energy band by the SGD in a 50 ks exposure time (courtesy Sasano).

Giant outbursts of Be/X-ray binaries are thought to be due to an exceptional extension of the equatorial disc of the donor star providing material to be accreted on the NS through a viscous accretion disc (see Reig,

2011, for a review). Outbursts are not predictable although a correlation is observed with the strength of the H- α emission of the system. In 4U 0115+63, these episodes happen every few years and appear to be linked to a semi-period perturbation of the equatorial disc of the Be donor (Negueruela et al., 2001). Longer periods of quiescence followed by repeated outbursts have been observed for A 0535+26, while EXO 2030+375 shows periodic outbursts at each periastron passage during which the source does not exceed ~ 250 mCrab. The spectacular source V 0332+53 has been observed in outburst only once with modern facilities. GRO J1008–57 has recently exhibited a giant outburst (Kuehnel et al., 2012). All these objects are potential targets for *ASTRO-H* in case they go in outburst. Triggers can be provided by *Swift*/BAT, *INTEGRAL*, or *MAXI* and the X-ray outbursts usually last for a few weeks.

Observations during these episodes would provide unprecedented data sets to study X-ray binaries. We emphasise that the SGD can measure X-ray polarisation above ~ 50 keV where cyclotron lines appear in a handful of very bright transient sources, for which we have simulated the feasibility of detection in different observing times (see Table 1). For the X-ray binary A 0535+26 ($E_{\text{cyc}} \simeq 45$ keV), at the maximum of its powerful out-

bursts (0.9 Crab above 50 keV) and in 25 ks of observation, it is possible to measure a polarisation fraction as low as 7%. In Figure 9, we show how this measurement would be possible throughout the outburst, helping us to contain the details of the emission mechanism at different luminosity levels. In systems as EXO 2030+375, in which the detection of a scattering feature is controversial, (Wilson et al., 2008; Klochkov et al., 2007, and references therein), it would be feasible to detect a polarisation fraction of 20% during the regular periastron passages, while 8% would be reachable if the source undergoes a giant outburst. This would constitute a direct prove of the magnetic field intensity even in absence and a clear spectral signature and would open a new window to investigate why the scattering features are not an ubiquitous phenomenon in magnetised pulsars.

The polarisation angle is strongly dependent on the B -field orientation with respect to the line of sight and averaging over a phase interval might lead to a lowering of the polarisation signal. We argue, based on a rough comparison of theoretical computations (Meszaros et al., 1988), that it could be sufficient to divide the pulse profile in less than ten phase bins to measure a polarisation fraction of a few 10% in most bins and it would thus be sufficient to invest a reasonable amount of observing time (100-200 ks) on a bright X-ray binary to achieve such a breakthrough result.

Table 1: Estimated minimum detectable polarisation fraction in the 50–100 keV energy range for bright Be/X-ray binaries.

Exposure (ks)	A 0535+26	GX 304–1	EXO 2030+375
25	7%	23%	8%
50	5%	16%	5%
100	3%	15%	4%

2.3 Super-giant Fast X-ray Transients (SFXTs)

2.3.1 Background and Previous Studies

Together with the classical supergiant and Be/X-ray binaries, the *INTEGRAL* satellite has provided evidence for a third class of X-ray binary called the supergiant fast X-ray transients (SFXTs) (Smith et al., 2004; Sguera et al., 2005; Negueruela & Smith, 2006). These objects have an OB supergiant donor star, but at odds with the persistent systems, they show short hours-long periods of intense X-ray activity (flare, $L_X \sim 10^{36-37}$ erg/s), often grouped in day-long outbursts, and extended quiescent states ($\sim 10^{32}$ erg/s), with swings up to 10^5 in luminosity (see, Romano et al., 2014, for an extensive summary). An open debate exists on the nature of the accreting object and the characteristics of the stellar wind from which matter is funnelled: clumpy winds are thought to cause the very variable accretion rate (in’t Zand, 2005; Walter & Zurita Heras, 2007; Rampy et al., 2009), but some gating mechanism is probably in action to produce the very low duty cycle of these objects compared to the classical systems (Oskinova et al., 2007; Grebenev & Sunyaev, 2007; Bozzo et al., 2008). The spectral characteristics of the objects and the detection of pulsation (from 20 to 1200 s, references in Romano et al., 2014) in five out of twelve confirmed systems strongly indicate that the compact object is a neutron star. It is therefore possible that the gating barrier is provided by an ultra-strong magnetic field ($B \gg 10^{12}$ G), which causes matter to accumulate or be expelled at the magnetospheric boundary. Evidence of flares linked to ingestion of clumps has been reported in *XMM-Newton* and *Suzaku* observations (Rampy et al., 2009;

Bodaghee et al., 2011; Bozzo et al., 2011), while the typical flare rise time (~ 10 min) is consistent with the free-fall time from the Alfvén radius associated to magnetic field $B \sim 10^{13}$ G.

2.3.2 *ASTRO-H* perspectives on SFXTs

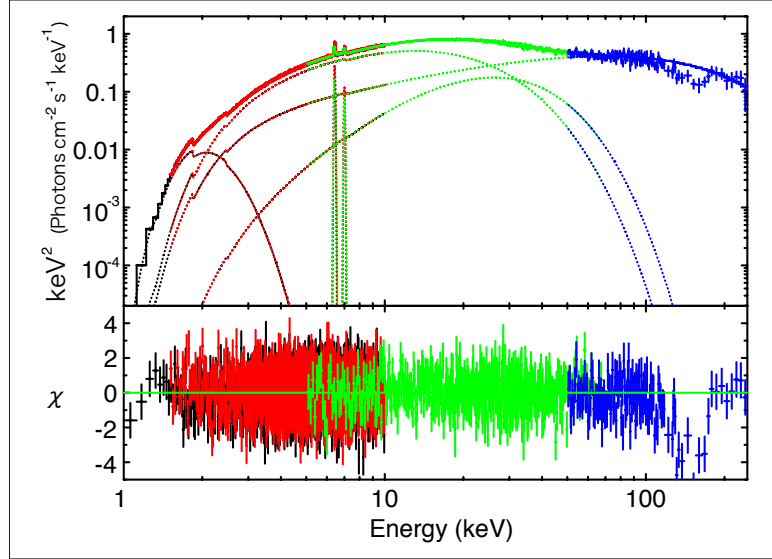


Figure 10: Top: Simulation of 100 ksec *ASTRO-H* observation of long period pulsar, 4U 0114+65, with a CRSF at 150 keV. Bottom: Residuals of the simulation against a model with no CRSF. The residuals clearly deviate from the model at ~ 150 keV and the CRSF will be sufficiently detectable with the SGD.

ASTRO-H will provide unprecedented tools to study the very nature of these objects. The HXI can provide good sensitivity to the presence of a cyclotron scattering absorption feature in the hard X-ray domain, with a possible extension using the SGD at higher energy for very bright events. The SXS can provide a very useful diagnostic on the presence of the emission Iron line, its ionisation status and the proper motion of the clump impacting on the NS. The absorption can be constrained by the SXI and SXS, similarly to the *Suzaku* achievements (Bodaghee et al., 2011; Rampy et al., 2009). Such objects, if confirmed, may be considered as aged magnetars in binary systems, and will provide clues to the formation and evolution of magnetars (Enoto et al., 2010), as well as to the origin of the NS magnetism (Makishima et al., 1999).

Other candidates to search for cyclotron scattering features are the long period pulsars (e.g., 4U 0114+65 and 4U 2206+54). Their spectrum extends to 100 keV without appreciable cut-off, unlike those of ordinary X-ray pulsars which show a steep cutoff around 20–40 keV and a CRSF at a higher energy. We thus expect these LPPs to exhibit CRSFs in energies above ~ 100 keV (Makishima et al., 1999), where the SGD will for the first time realize a sufficient sensitivity.

2.4 Gamma-ray Loud Binaries

2.4.1 Introduction

Gamma-ray-loud binary systems (GRLB) are X-ray binaries which emit very-high energy (VHE) γ -rays. Four such systems PSR B1259–63, LS 5039, LSI +61° 303 and HESS J0632+057, have been firmly detected as persistent or regularly variable TeV γ -ray emitters (Aharonian et al., 2005, 2006a; Albert et al., 2006; Aharonian et al., 2006b).

Observations of the *Fermi*/LAT telescope helped to reveal several more binaries emitting at very high energies. Among these sources are well-known microquasar Cyg X-3, symbiotic binary V 407 Cygni, colliding

wind binary η Carina, newly discovered binary system 1FGL J1018.6-5856, but still the number of known GRLBs is very limited.

The source of the high-energy activity of GRLBs is uncertain. It can be either accretion onto or dissipation of rotation energy of the compact object. It is commonly assumed that the γ -ray emission is produced in result of interaction of the relativistic outflow from the compact object with the non-relativistic wind and radiation field of a companion massive star. Neither the nature of the compact object nor the geometry and physical properties of relativistic wind from this compact object are known in most of the GRLBs. The only exception is PSR B1259–63 system in which the compact object is known to be a young rotation powered pulsar which produces relativistic pulsar wind.

In Bednarek (2009) it was proposed that accreting magnetars in massive binaries can also generate TeV gamma-rays. In the inner magnetosphere of a magnetar the magnetic pressure can balance the gravitational pressure of the accreting matter, creating a very turbulent, magnetised transition region. This region provides good conditions for acceleration of electrons to relativistic energies. These accelerated relativistic electrons lose energy on the synchrotron process and the Inverse Compton scattering of the radiation from the nearby massive stellar companion, producing high energy radiation from X-rays up to TeV γ -rays.

Recently Burst Alert Telescope (BAT) on board *Swift* has detected a short burst from the direction of the TeV binary LSI +61° 303. The burst is visible in the 15 - 50 keV energy range, while no significant excess is observed above 50 keV. The total duration of the event is about 0.3 s. Previously such short flares have been also observed from the direction of LSI +61° 303 by *RXTE* (Smith et al., 2009; Li et al., 2011). In the paper of Torres et al. (2012) it was noticed that the properties of the burst observed by *Swift*/BAT (a very short duration and a thermal spectrum) are typical of magnetars. In their work the authors propose that due to the highly eccentric orbit the system is subject to flip-flop behaviour, from a rotationally powered regime in apastron to a propeller regime in the periastron. In this case in apastron an interwind shock leads to the normally observed LSI +61° 303 behaviour, while during the periastron propeller is expected to efficiently accelerate particles only to sub-TeV energies, in agreement with the observations.

More observations are needed to find out the true nature of these very interesting systems. Below we discuss how *ASTRO-H* observations could help to solve some unresolved problems. We start with the case of PSR B1259–63, the only system in which we are sure about the nature of the compact object, and which we can use as a sample to test the other systems. Study of this system could provide a clue on the energy of the relativistic particles of the pulsar wind and give us a chance to study interactions of the winds in the highly variable environment. After that we discuss in more details LSI +61° 303 and show the importance of measuring of its spectral variability in a broad energy range (1 - 100 keV) along the orbit.

2.4.2 PSR B1259-63

In PSR B1259–63 a 48 ms radio pulsar is in a highly eccentric 3.4 year orbit with a Be star LS 2883. This system is known to be highly variable on an orbital time scale in radio (Johnston et al. 2005 and references therein), X-ray (Chernyakova et al. 2009 and references therein), and TeV (Aharonian et al., 2005) energy ranges. The orbital multi-wavelength variability pattern is determined by the details of the interaction of relativistic pulsar wind with a strongly anisotropic wind of the companion Be star, composed of a fast, rarefied polar wind and a slow, dense equatorial decretion disk. The disk of the Be star in the PSR B1259–63 system is believed to be tilted with respect to the orbital plane. The line of intersection of the disk plane and the orbital plane is oriented at $\sim 90^\circ$ with respect to the major axis of the binary orbit (Wang et al., 2004) and the pulsar passes through the disk twice per orbit.

Despite the intensive observational campaigns during the last three periastron passages (2004, 2007 and 2010) it was still not possible to conclude whether the observed X-ray emission has inverse Compton or synchrotron origin (Chernyakova et al., 2009). The answer to this question is very important for our understanding of the composition of the pulsar wind, as the Lorentz factor of the relativistic electrons varies from about 10 to 10^6 in these two models. Study of the variability of the broad band (1 – 100 keV) spectrum of the source as the pulsar interacts with the disk before and after the periastron could give the missing clues to answer this question.

Suzaku observations of the 2007 periastron passage show a break of the source spectrum as the pulsar was crossing the disk before the periastron (Uchiyama et al., 2009), see left panel of Figure 11. However presence of the nearby X-ray pulsar IGR J13020-6359, located only 10 minutes from the PSR B1259–63 makes the results of *Suzaku*/HXD very model dependent, and independent measurements in this energy range with the imaging instrument would be a huge benefit. Right panel of Figure 11 show simulation of 10 ks observation of PSR B1259–63 with *ASTRO-H*. On this Figure we model the broken power law slope as observed with *Suzaku*. On the left Figure we show that if one would try to fit such a spectrum with a single power law the high energy data will clearly deviate from the model.

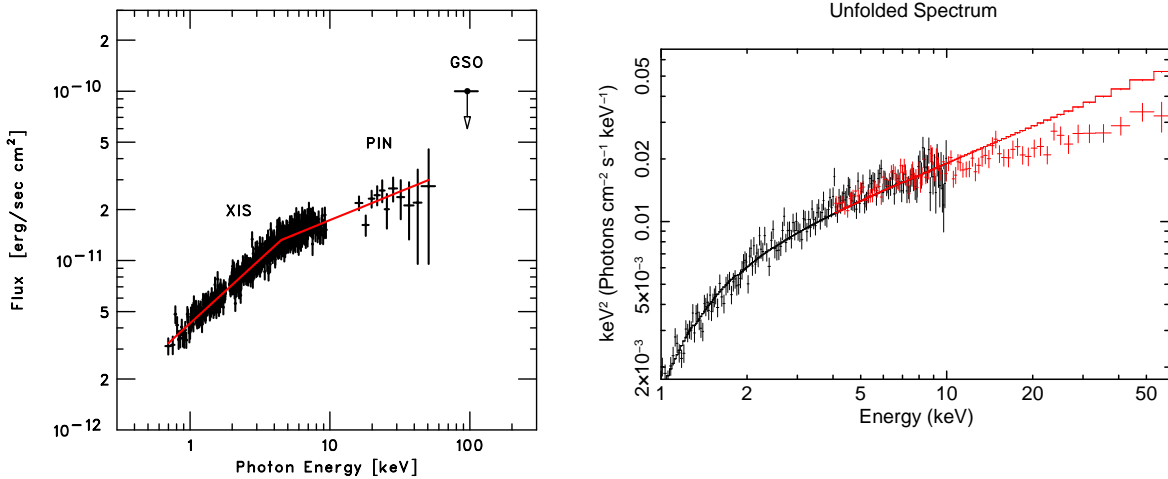


Figure 11: *left panel:* *Suzaku* observations of the spectral break in PSR B1259–63. Figure is taken from Uchiyama et al. (2009). *right panel:* Simulation of 10 ksec *ASTRO-H*/HXI observation of PSR B1259-63 as it crosses the disk with the parameters derived from the *Suzaku* observation. Fit with a single power law leads to the clear deviation of the data from the model.

2.4.3 LSI +61 303

The Be star binary LSI +61° 303 is another GRLB system from which radio, X-ray and very high-energy gamma-ray emission is observed. In LSI +61° 303 the high-energy particle outflow is directly observed in the radio band, where angular resolution is sufficient to resolve the source and to detect variations of its morphology on the orbital period time scale. The observed morphological changes indicate that the outflow has a variable morphology outflow filling a region the size $\sim 10^2 - 10^3$ times larger than the binary separation distance. The radio signal could not be used to trace the outflow down to the production site inside the binary orbit, because of the free-free absorption in the dense stellar wind environment (Zdziarski et al., 2010). To understand the nature of the high-energy particles carrying outflow one has to use complementary high-energy data in X-ray and/or γ -ray bands.

Two major types of models of radio-to-X-ray activity of LSI +61° 303 were proposed in the literature. Models of the first type assume that activity of the source is powered by accretion onto the compact object. Alternatively, the activity of the source could be explained by an interaction of a young rotation powered pulsar with the wind from the companion Be star.

If the system is an accreting neutron star or black hole, one expects to find a cut-off powerlaw spectrum in the hard X-ray band. The cut-off energy is normally at 10 – 60 keV for neutron stars and at ~ 100 keV for black holes. If the jet and accretion contributions to the X-ray spectrum are comparable, then emission from the accretion disk should at least produce an observable spectral feature (e.g. a bump, a break or turnover) in the 10-100 keV energy band.

Currently the hard spectrum of LSI +61° 303 was checked only with the *INTEGRAL*. Unfortunately the source is rather weak for the *INTEGRAL* and the only possibility to measure the spectrum was to sum up spectra collected through the years of observations. The resulted spectra didn't show a break, but have indicated

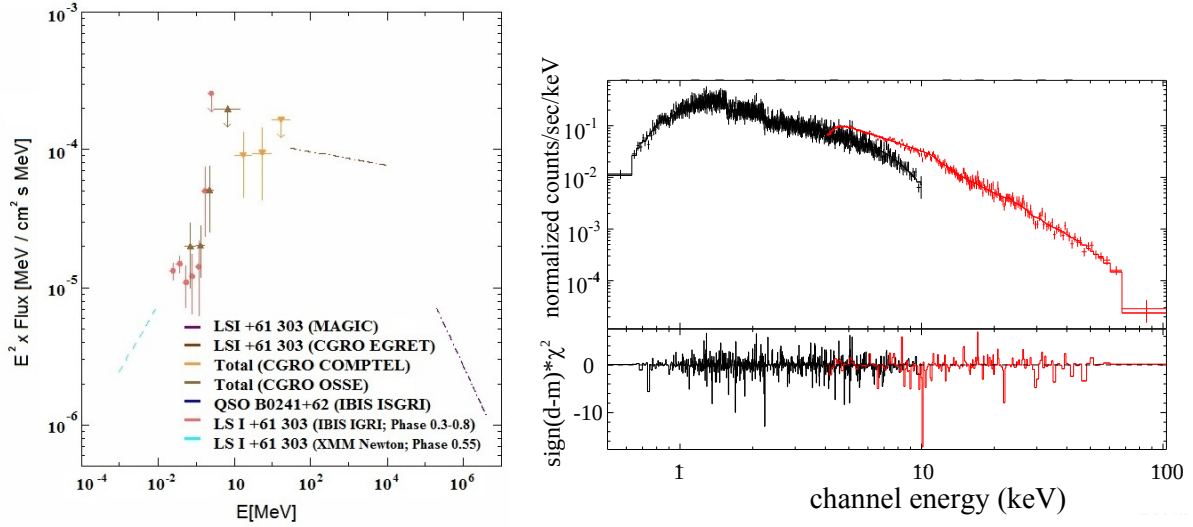


Figure 12: *left:* Broad band spectrum of LSI +61° 303. *INTEGRAL* observations reveal a presence of a possible feature at 50 keV. Figure is taken from W. Hermsen and L. Kuiper presentation at the first *Fermi* Symposium. *right:* Simulation of 40 ks *ASTRO-H* observation of LSI +61° 303.

a possible feature at around 50 keV, see left panel of Figure 12 presented by W. Hermsen and L. Kuiper at the first *Fermi* Symposium. Current *Suzaku* observations of the source are unable to constrain the spectrum of LSI +61° 303 above 50 keV. Clearly more sensitive observations are needed to clarify the nature of the source, and *ASTRO-H* observations can help to solve the issue, see right panel of Figure 12. On this panel we simulate a powerlaw spectrum with $N_H = 0.5 \times 10^{22} \text{ cm}^{-2}$, $\Gamma = 1.5$ and $F_{2-10} = 1.2 \times 10^{-11} \text{ erg cm}^{-2} \text{ s}^{-1}$.

3 Probes into Magnetars and their Environment

3.1 What makes magnetars and how do they evolve? Probing their supernova progenitors, energetics and evolution

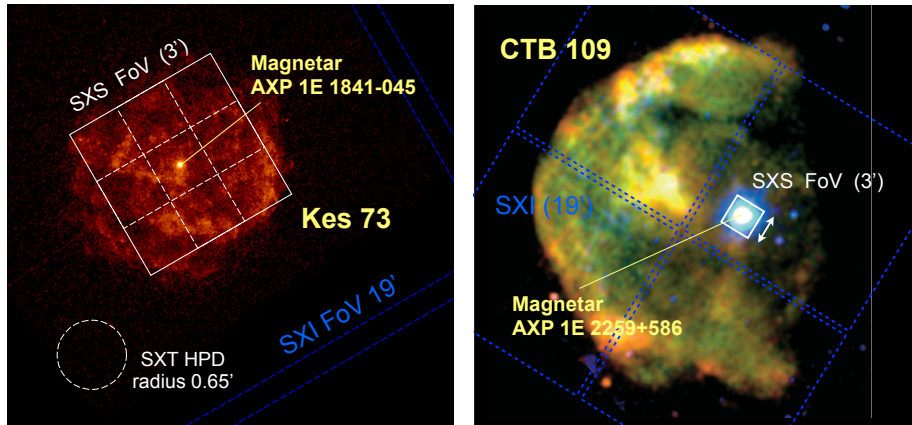


Figure 13: Bright magnetar SNRs: (left) The young SNR Kes 73 observed with *Chandra* with *ASTRO-H*'s SXS and SXI fields of view overlaid. The central source is the AXP 1E 1841–045. (right) The evolved SNR CTB 109 with *XMM-Newton* (Sasaki et al., 2004) with *ASTRO-H*'s SXS and SXI field of views. The central source is the AXP 1E 2259+586. The dim western half part of this SNR is covered by a giant molecular cloud.

The different manifestations of neutron star classes (see §1 and Figure 1) can be potentially linked to the different environments and progenitors of the supernova explosions creating these compact objects. While there

is currently no general consensus on the progenitors of highly magnetized neutron stars (including the high-magnetic field radio pulsars and magnetars), there is accumulating evidence, using multi-wavelength studies, for them to originate from very massive progenitors, i.e. with mass $\gtrsim 20$ solar masses, and expanding into a relatively low-density medium; see Safi-Harb & Kumar (2013) for a summary. X-ray spectroscopy of their associated supernova remnants (SNRs) is particularly a powerful tool in inferring their progenitor mass through the detection of the X-ray emitting ejecta and comparison to nucleosynthesis models (see the *Young Supernova Remnants* White Paper (WP#7) for a more detailed discussion of this). If indeed magnetars originate from very massive progenitors, as can be diagnosed with X-ray spectroscopic studies of their associated SNRs, then this will lead to the much interesting implication that very massive stars do *not* necessarily form black holes.

To date, only a handful SNRs are associated with magnetars, while the majority of the ~ 330 known Galactic SNRs are associated with rotation-powered neutron stars or other subclasses of neutron stars (Safi-Harb, 2013; Ferrand & Safi-Harb, 2012). While this sparse SNR-magnetar association by itself holds some clues on the nature of these objects, studying the energetics and properties of their associated SNR emission further addresses the magnetar nature of these sources. In particular, one popular model for magnetars is that they are formed from proto-neutron stars with initial spin periods of only $\sim 0.6\text{--}3$ ms. The combination of convection and fast rotation helps build up the magnetic field to ultra-high values during the first tens of seconds following neutron star birth (Duncan & Thompson, 1992, 1996). Such initial fast spin periods would imply larger-than-typical initial rotational energy of the neutron star, which in turn would lead a more energetic SNR. Past and current X-ray spectroscopic studies, however, indicate that the SNRs associated with highly magnetized neutron stars appear to have typical supernova kinetic energies in the $10^{50}\text{--}10^{51}$ ergs (Vink & Kuiper, 2006; Vink, 2008; Safi-Harb & Kumar, 2013), posing a challenge to the proto-neutron star model for magnetars. Furthermore, more recent estimates for the explosion energies in two SNRs hosting an anomalous X-ray pulsar (Kes 73/AXP 1E 1841–045) and a high magnetic field radio pulsar (G292.2–0.5/PSR J1119–6127) (Kumar et al., 2014, 2012) confirm these “typical” explosion energies. These studies also propose very massive progenitors ($\gtrsim 20$ solar masses) based on the X-ray spectroscopic studies of these SNRs with *Chandra* and *XMM-Newton*.

The past and current X-ray studies with *Chandra*, *XMM-Newton*, and *Suzaku* have been however severely limited by poor statistics and the lack of spectral resolution and sensitivity needed for a more appropriate study and modelling of the X-ray emitting supernova ejecta and surrounding medium. Such an analysis can be best performed with the SXS on-board the *ASTRO-H* satellite. Together with its coverage in the hard X-ray band thanks to the Hard X-ray Imager and the Soft Gamma-ray Dectector, *ASTRO-H* will provide a unique window to study *simultaneously* the thermal plasma associated with the SNR, and the associated compact objects with spectra characterized by both both a soft and a hard X-ray component and which occasionally emit outbursts that should impact their “beambags”, i.e. their associated SNRs.

The SNR Kes 73 hosting the AXP 1E1841-045 represents an ideal magnetar-SNR for *ASTRO-H* given its brightness, size, and previous detailed X-ray studies of both the SNR and AXP with CCD-type spectra. In Figure 14, we show the SXS field of view overlaid on the SNR, with the pointing aimed at covering the brightest and bulk of X-ray emission from the SNR, while also covering the AXP. Figure 14 shows a 100 ks SXS simulated spectrum of the diffuse emission from the SNR emission fitted with a two-component non-equilibrium ionization model based on the *Chandra* and *XMM-Newton* study (Kumar et al., 2014). The CCD spectrum shows evidence for a soft, ejecta-dominated component, and a hot, low-ionization timescale component, attributed to the shocked ISM or CSM blown by a massive progenitor. The simulated spectrum will provide new constraints on the ejecta abundances, and thus on the mass of the progenitor star through a comparison to nucleosynthesis model yields such as those of Woosley & Weaver (1995) and Nomoto et al. (2006). As well, the Fe-K line complex will provide the first opportunity to diagnose the hot plasma conditions and confirm or refute the stellar wind blown bubble scenario.

The right panel of Figure 14 shows the simulated broadband (SXS+HXI+SGD) spectrum of the central AXP 1E 1841–045, illustrating the additional magnetar science that can be done with the same observation. While the line emission from the SNR dominates in the SXS band, the AXP’s spectrum dominates in the hard band (HXI+SGD). In particular, the spectrum will shed light on a) the magnetic field of the AXP through a confirmation of the ~ 30 keV cyclotron (emission or absorption) feature detected recently with *NuSTAR* (An

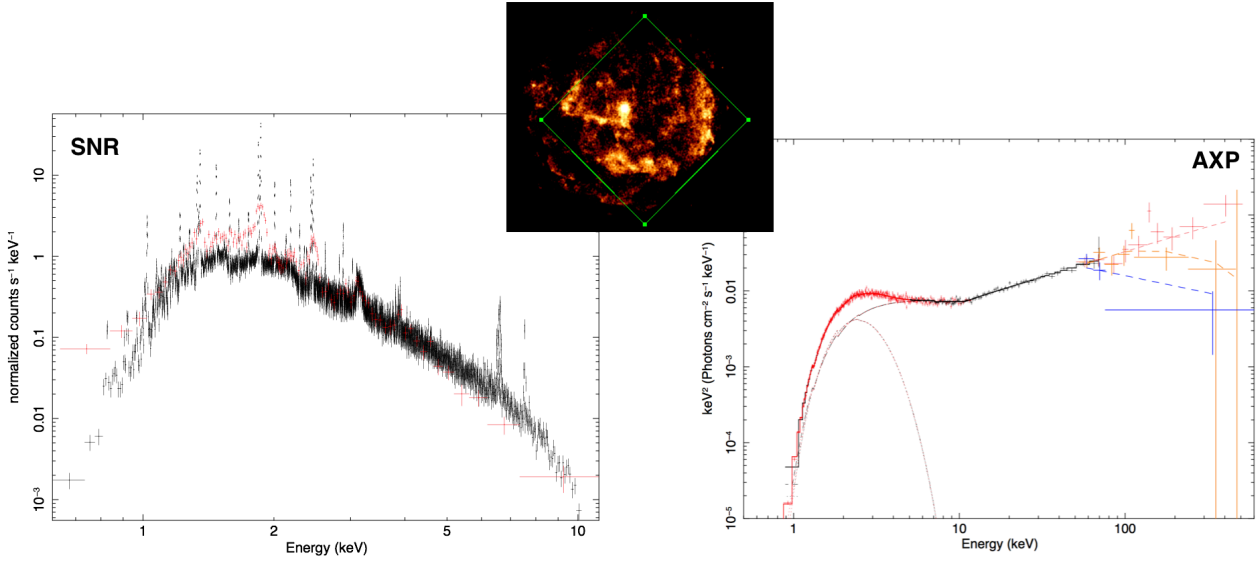


Figure 14: Simulated spectra for the SNR Kes 73 and its associated AXP 1E1841–045 shown using a *Chandra* observation (Kumar et al., 2014) with *ASTRO-H*’s SXS field of view overlaid. (Left) A 100 ksec SXS simulation of the SNR Kes 73 (with the AXP’s spectrum excluded) obtained using *simx*, shown in comparison with the *XMM-Newton* MOS1 spectrum. The SXS spectrum should allow us to resolve the line emission (particularly from the Mg, Si and S complex) and detect for the first time strong line emission from Fe-K. This will be needed to constrain the abundances and thus the mass of the progenitor star. (Right) Shown next for comparison the broadband SXS+HXI+SGD 100 ks simulated spectrum of the AXP 1E 1841–045 associated with the SNR Kes 73. In the SGD band, we assumed three possibilities: no spectral break (red), a roll-over in the SGD band (orange), and a steep cutoff just above the HXI (or *NuSTAR*) energy band. Studying both the SNR and the AXP with *ASTRO-H* will provide the first broadband view of this system. We note that the AXP’s total flux is $\sim 10\%$ that of the SNR’s flux in the SXS band. The AXP’s emission won’t affect the line diagnosis of the SNR for abundance studies, but will dominate the continuum in the hard X-ray band.

et al., 2013), and b) the nature of the hard X-ray emission through pinning down the spectral cutoff with the HXI+SGD combined spectrum. If the 30 keV feature is attributed to a cyclotron line, the magnetic field is estimated to be 3×10^{12} G (electron cyclotron) and 5×10^{15} G (proton cyclotron). Furthermore, so far we have not yet distinguished between the competing theoretical models for the origin of the magnetar’s hard X-ray emission. For example, the e^+/e^- -outflow model (Beloborodov, 2013) predicts the ν - F_ν peak at ~ 7 MeV (An et al., 2013) while the fall-back disk predicts it at ~ 100 – 200 keV (Kylafis et al., 2014). This will be an advantage over *NuSTAR* due to the sensitivity of *ASTRO-H* above 70 keV. This science will be further discussed in Sections 3.2 and 3.3.

CTB 109 is another relatively bright, but more evolved, SNR associated with a magnetar, AXP 1E2259+586 (see Figure 13). The remnant appears as a half-shell due to an obscuring molecular cloud on the western side. A most recent study with *Chandra* showed the presence of shock-heated ejecta with enhanced Si and Fe in and around the lobe adjacent to the AXP. The lobe is believed to be created by the interaction of the SNR shock wave and the supernova ejecta with a dense and inhomogeneous medium in the SNR environment (Sasaki et al., 2013). In Figure 15, we show a simulated 100 ksec SXS spectrum based on a *Suzaku* observation, illustrating the wealth of lines that will be resolved with SXS.

One of the puzzling questions about magnetar SNRs is the discrepancy between the SNR’s age (normally estimated from the shell’s shock velocity) and the magnetar’s age (estimated from the characteristic age of the pulsar, $P/(2\dot{P})$). This discrepancy is particularly pronounced for the SNR CTB 109 (Sedov-estimated age ~ 13 – 17 kyr) and its AXP 1E 2259+586 (~ 230 kyr), as recently confirmed with *Chandra* (Sasaki et al., 2013) & *Suzaku* observations (Nakano et al., accepted). The answer to this puzzle lies in understanding how magnetic fields evolve in magnetars and in acquiring accurate measurements of the associated SNR’s shock velocity.

Giant flares, short bursts, and bright persistent X-ray emission exceeding the spin-down power are thought

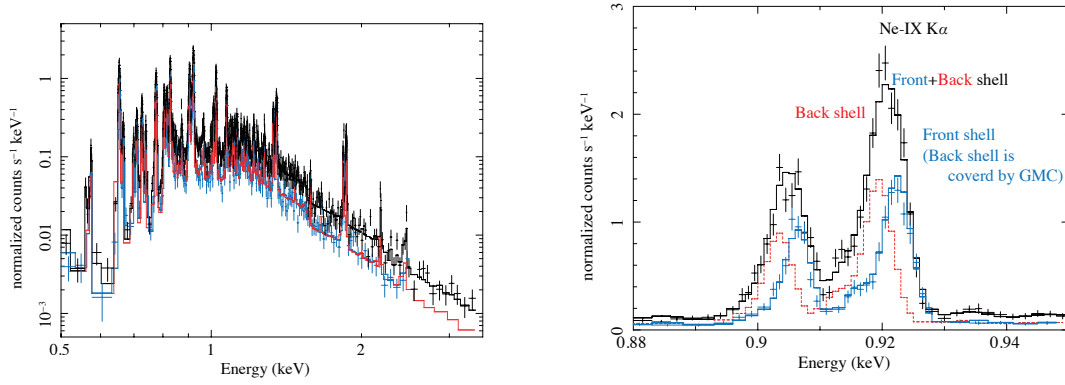


Figure 15: (left) A 100 ks SXS simulated spectrum of the SNR CTB 109 using a two-component absorbed non-equilibrium ionization model based on the *Suzaku* data. (right) SXS simulation of the Ne-IX lines based on the *Suzaku* spectra. Red- and blue-shifted lines and their sum are shown in red, blue, and black colors, respectively. Depending on the pointing position, we can observe both shell components (black) or only the front shell (blue), since the shell at far-western side is covered by the giant molecular cloud.

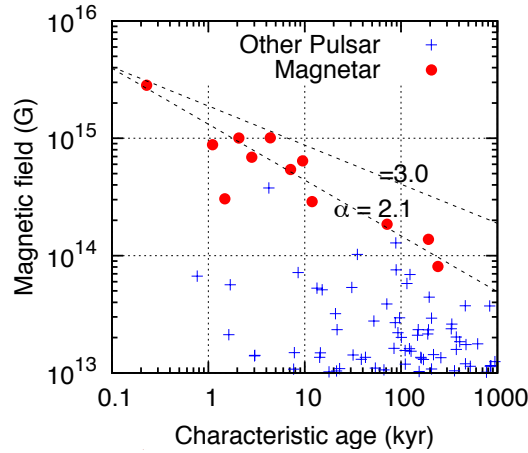


Figure 16: Magnetic field of magnetars and other (rotation-powered) pulsars calculated from the pulsar's period and its derivative (Nakano et al., submitted).

to originate from the magnetic energy dissipation. However, how the magnetic field of magnetars evolves with time, as the magnetar ages, is still being debated. The magnetic field measured from P and \dot{P} is known to decrease with the characteristic age, $P/(2\dot{P})$, as illustrated in Figure 16.

While large characteristic ages can be potentially explained if one accounts for the magnetic field decay in magnetars (Colpi et al., 2000), the age measurement of associated SNRs provides an independent way of understanding the magnetic field evolution. This can be done through an accurate measurement of the shock velocity, which will be also useful for probing the supernova explosion energy shedding light on the origin of magnetars. For example, in the Sedov phase of SNR evolution, the explosion energy and age are given by $E \propto R^3 v^2$ and $\tau_{\text{SNR}} = 5R/2v$, respectively. For the SNR CTB 109, the large molecular cloud on the western side is blocking half of the shell on the far-side while the shell is fully visible on the eastern side. As a result, depending on the pointing direction, SXS is expected to measure blue- and red- shifted lines originating from expanding shells towards and away from us. The 100 ks SXS simulation in Figure 15 assumes a velocity of 500 km s^{-1} , inferred from the *Chandra* observation of CTB 109 (Sasaki et al., 2013). The Doppler shift of the Ne-IX K lines can be detectable, and simultaneous usage of multiple lines in the soft band increases the accuracy of the measurements. For the compact object, we will be able to address its magnetic field strength and probe its hard X-ray emission, as detailed in Sections 3.2 and 3.3.

In summary, the young and more evolved SNRs Kes 73 and CTB 109, respectively hosting the magnetars

1E 1841–045 and 1E 2259+586 at their centers, cover all the fundamental questions presented in this white paper (see the next sections for the compact objects’ science). The same method can be also applied to the other handful magnetar SNRs. This science is also relevant to WP#7.

3.2 Can we find direct evidence of the strong field?

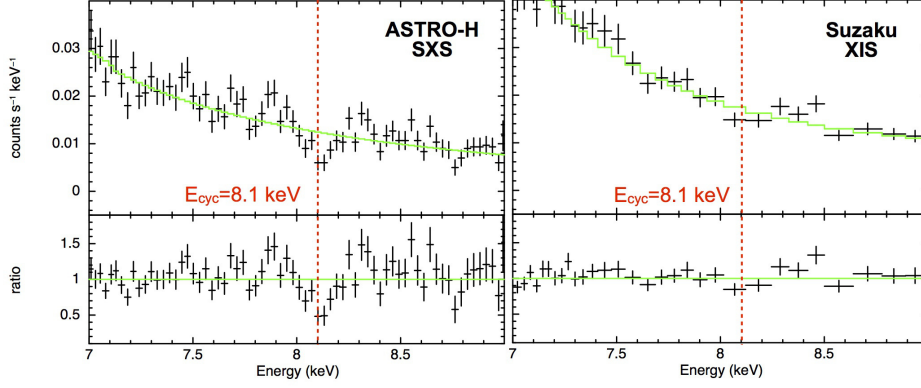


Figure 17: Simulated possible proton CRSF at $E_{\text{cyc}} = 8.1$ keV of *ASTRO-H*/SXS (left) and of *Suzaku*/XIS (right). Both Monte Carlo simulations employ the same model, assuming a 100 ksec exposure and a Gaussian feature on the continuum observed in 4U 0142+61, with a line width $\sigma_{\text{line}} = 40$ eV and an equivalent width of 60 eV.

In the strong magnetic field ($B > B_{QED}$) of magnetars, the electron cyclotron resonance scattering feature (CRSF) falls above the MeV range, while the proton CRSF (Eq. 1) falls right in the soft X-ray band. The dipole magnetic fields derived from P and \dot{P} reflects only from the poloidal component; this CRSF can provide a direct determination of the total surface B -field. Early theoretical predictions suggested that the proton CRSF exhibits an equivalent width up to many hundred eV and a relatively wider absorption width of $\Delta E/E_{pc} \sim 0.05 - 0.2$ (Ho & Lai, 2001; Zane et al., 2001). Contrary to expectations for the detection of proton cyclotron lines as a direct measurement of the strong B -field, there are quite a few observational reports of the proton CRSF so far from the quiescent magnetar spectra: $\sim 5, 10$ keV from 1E 2259+586 (Iwasawa et al., 1992), ~ 8.1 keV from 1RXS J1708-4009 (Rea et al., 2004), and more recently an absorption feature from SGR 0418+5729 (Tiengo et al., 2013) and a 25–35 keV (absorption or emission) weak feature from 1E 1841-045 in the SNR Kes 73 (An et al., 2013). Some of those have not yet been confirmed by following observations (Rea et al., 2007; Malygin & Iakubovskiy, 2011). In the absence of a significant CRSF in most of the quiescent X-ray spectra of magnetars, it was pointed out that vacuum polarization effectively suppresses the strength of the proton CRSF, making the equivalent width nearly an order of magnitude lower than previously thought (Lai & Ho, 2002; Özel, 2003). In addition, the gradient of the B -field and effective temperatures would suppress these features as well. *ASTRO-H*’s SXS, combined with its broadband capability with HXI+SGD, will allow us to test for this and confirm previously reported features.

More puzzling, some proton CRSF have been reported from bursts spectra, as shown in table 2; e.g., at 5.0, 11.2, and 17.5 keV of SGR 1806–20 with *RXTE* (Ibrahim et al., 2002, 2003). Even though the number of detections in bursts is larger than that of the persistent emission, these detections are still quite rare compared to numerous short bursts from magnetars. In summary, the current observations have not yet achieved a consistent interpretation of the proton cyclotron features, requiring much deeper observations by high-resolution instruments.

The Soft X-ray Spectrometer (SXS) on board *ASTRO-H* can provide a higher sensitivity search for the proton CRSF even with a shallower and/or narrower width than the previous studies. Since the previous persistent and burst observations have not yet provided a consistent picture of the proton CRSF (e.g., resonance energy, absorption width, equivalent width, and spectral shapes), here we empirically assume the possible Gaussian absorption feature, and simulate the sensitivity to detect the lines. Figure 17 shows Monte Carlo simulations of the absorption feature at 8.1 keV from the anomalous X-ray pulsar 4U 0142+61. As shown in this plot,

Table 2: Reported absorption-like features in magnetars, with reference to (Malygin & Iakubovskiy, 2011).

Object	E_{pc} (keV)	Detector	Note	Ref.
SGR 1806-20	5.0, 7.5, 11.2, 17.5	<i>RXTE/PCA</i>	in the harder part of a precursor	(1) (2)
SGR 1900+14	6.4	<i>RXTE/PCA</i>	during precursor to the main burst	(3)
1RXS J1708-4009	8.1	<i>BeppoSAX</i>	the longest observation (200 ks) during rising phase	(4) (5) (6)
1E 1048.1-5937	14	<i>RXTE/PCA</i>	emission, in a burst	(7)
...	13	<i>RXTE/PCA</i>	emission, at one part of a burst tail	(8)
XTE J1810-197	12.6	<i>RXTE/PCA</i>	emission in a burst tail	(9)
4U 0142+61	4, 8, 14	<i>RXTE/PCA</i>	emissions, in the most energetic among a sequence of bursts	(10)
1E 2259+586	5, 10	<i>Ginga/LAC</i>	during flux increase	(11)
1E 1841-045	25–35	<i>NuSTAR</i>	phase-resolved spectrum	(12)

References: (1) Ibrahim et al. 2002, (2) Ibrahim et al. 2003, (3) Strohmayer & Ibrahim 2000, (4) Rea et al. 2003, (5) Rea et al. 2004, (6) Oosterbroek et al. 2004, (7) Gavriil et al. 2002, (8) Gavriil et al. 2006, (9) Woods et al. 2005, (10) Gavriil et al. 2008b, (11) Iwasawa et al. 1992, (12) An et al. 2013

compared to the XIS on board *Suzaku*, the high resolution of the SXS would allow the detection of weaker features (small equivalent width). Figure 18 represents an example of detectability of the proton CRSF on the equivalent width versus energy plane. Comparing to the previous *XMM-Newton* observations, the SXS potentially search for features with a factor of 2–3 weaker equivalent width.

3.2.1 On the link between magnetars and the other classes of neutron stars through a direct measurement of the magnetic field

As mentioned in Section 1, the growing diversity of neutron stars includes an intriguing class of compact objects near the centres of core-collapse SNRs, referred to as CCOs (for Central Compact Objects). These objects are typified by the CCO discovered with the first light *Chandra* observation of the O-rich supernova remnant (SNR) Cas A. Originally, CCOs were thought to be “relatives” of magnetars primarily based on the resemblance between their X-ray spectra in the 0.5–10 keV band, the relatively slow spin periods (in comparison to the typical rotation-powered pulsars), and the lack of radio emission and pulsar wind nebulae surrounding them.

Recent dedicated timing observations of a few CCOs led to the suggestion that these are “anti-magnetars”, i.e. with a magnetic field much smaller than a typical magnetar’s field, with inferred $B \sim 10^{10} - 10^{11}$ Gauss; see Gotthelf & Halpern (2009) for the discovery of a 112 ms period in the CCO residing in the SNR Puppis A. The measured \dot{P} implies a surface dipole magnetic field $B < 9.8 \times 10^{11}$ G, most recently refined to a value of 2.9×10^{11} Gauss (Gotthelf et al., 2013). Evidence is accumulating for other low- B CCOs being anti-magnetars: 1E 1207.4–5209 in PKS 1209–51/52 and CXOU J185238.6+004020 in the SNR Kes 79. In addition to timing measurements, X-ray spectroscopic studies of the CCO in Cas A also supports the low- B scenario (Ho & Heinke, 2009). This study further indicates that the neutron star in Cas A is covered with a non-magnetized atmosphere of Carbon, the product of nuclear burning of H and He. Other, more exotic (quark star), models have been however proposed (Ouyed et al., 2014), in light of the recent *NuSTAR* study of the Cas A SNR (Grefenstette et al., 2014).

As for magnetars, a direct measurement of the CCOs magnetic field comes from cyclotron resonance lines, and such low B ($\sim 10^{10} - 10^{11}$ Gauss) are expected to show cyclotron features in the soft X-ray band, making the SXS an ideal instrument to study these features. Indeed cyclotron features have been discovered in a handful CCOs, including Puppis A’s CCO, RXJ 0822.0–4300, whose spectrum displays a phase dependent emission feature at 0.7–0.8 keV. This feature has been modelled either as an emission line of energy ~ 0.75 keV (hereafter emission) or as a cyclotron absorption feature plus a harmonic with an energy of $E_0 \sim 0.46$ keV, hereafter cyclotron (Gotthelf et al., 2013). It wasn’t possible to distinguish between these models using *Chandra* and *XMM-Newton* data. In Figure 19, we illustrate the capability of the SXS in differentiating between the emission model and the cyclotron model using a 100 ksec exposure. This particular CCO was selected

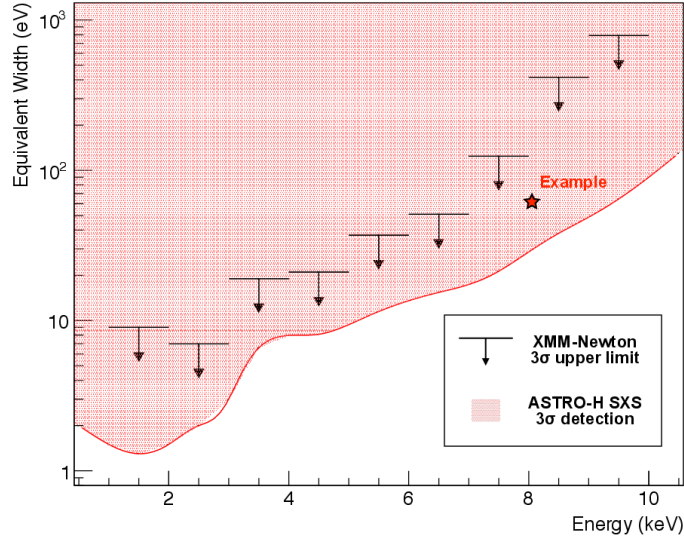


Figure 18: Detectable absorption features from the AXP 4U 0142+61. Feasibility to detect them ($>3\sigma$ detection region) in an *ASTRO-H* SXS 100 ksec observation are evaluated through the F-test probability with and without absorption features onto the X-ray continuum of 4U 0142+61. Gaussian absorption features are assumed at its width $\sigma_{\text{line}}=40$ eV. The previously measured energy-dependent 3σ upper limits are also shown as arrows referring to the 46 ksec *XMM-Newton* observation in 2004 (Rea et al., 2007), where assuming its possible absorption width at $\sigma_{\text{line}}=100$ eV. The star mark corresponds to Figure 17.

based on its location near the centre of a large and not so bright SNR (in comparison for example to Cas A’s CCO which will be difficult to resolve from the surrounding bright thermal emission from Cas A). We note however that this simulation does not take into account the presence of the SNR thermal plasma. This is meant as an illustrative example to show SXS’s capability to differentiate the different models proposed from fitting CCD-type spectra. Other more “isolated” targets (including other classes of neutron stars shown on Figure 1) with possible links to magnetars would be less contaminated by the X-ray emission from the SNR plasma.

In summary, SXS will open a new window to probe and understand the spectral features in an emerging and new class of (soft) X-ray emitting neutron stars, and confirm whether they are indeed anti-magnetars or descendants of magnetars.

3.3 Unified understanding of the magnetar X-ray spectrum?

The Hard X-ray component (HXC) was discovered from some magnetars above 10 keV by *INTEGRAL* and *RXTE* (Kuiper et al., 2006), and further confirmed by *Suzaku*. The HXC is distinguished from the well known soft X-ray component (SXC) since the HXC is represented by a power-law (PL) with an extremely hard $\Gamma_h \sim 1$, and extending >100 keV. The *CGRO/COMPTEL* and *Fermi/LAT* upper-limits (Abdo et al., 2010) suggest that the HXC must have a spectral break under ~ 750 keV which has not yet been clearly detected. The break energy is an important hint to constrain the emission mechanism of the HXC; e.g., thermal bremsstrahlung, synchrotron radiation and resonant Compton up-scattering (Thompson & Beloborodov, 2005; Baring & Harding, 2007). This is a unique science goal for the HXI and SGD.

In the *Suzaku* era, the simultaneous spectroscopy of the SXC and HXC revealed a possible broadband spectrum evolution; the hardness ratio, defined as F_h/F_s , is positively (or negatively) correlated with their magnetic field (or pulsar characteristic age). The Γ_h of the HXC is anti-correlated with the characteristic age. Although the interpretation of these correlations has not yet been established, one possible explanation is a down-cascade of the sub-MeV photons through photon splittings. Sub-MeV photons can be generated via electron-positron annihilation or resonant Compton up-scattering near the stellar surface, and are repeatedly splitting into hard X-rays in the QED field. In addition, Nakagawa et al. (2011) suggested a similarity of the hard X-ray spec-

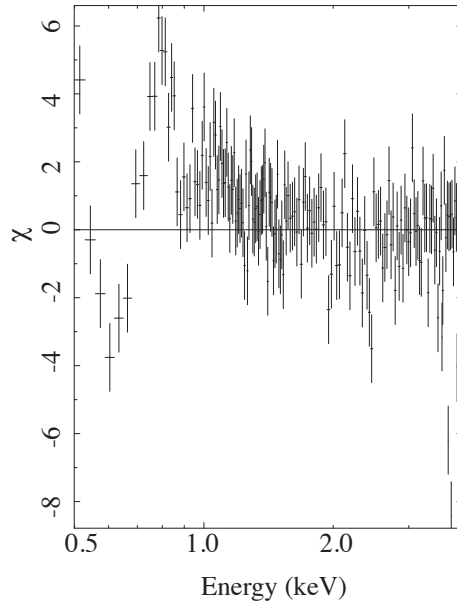


Figure 19: A 100 ksec SXS simulated spectrum of a CCO using a two-blackbody model plus an emission line, fitted with a two-blackbody model plus two cyclotron lines. The residuals illustrate the difference between proposed models that can be addressed with the SXS. We acknowledge the contribution of Adam Rogers (U. Manitoba) for this figure.

trum between the persistent emission and an accumulated weaker short bursts from the activated magnetar, SGR 0501+4516 (§3.4).

Furthermore, the broad-band coverage both of SXC and HXC can potentially provide a clue for the hidden toroidal magnetic field inside magnetars. In the recent *Suzaku* observation Makishima et al. (2014), an evidence for a free precession was detected from a prototypical magnetar 4U 0142+61. In the 15–40 keV hard X-rays, its 8.69 sec pulsations suffered slow phase modulations by 0.7 sec, with a period of ~ 15 h. When this is interpreted as free precession of the magnetar, the object is inferred to deviate from spherical symmetry by $\sim 1.6 \times 10^{-4}$ in its moments of inertia. This deformation, suggests a strong toroidal magnetic field, $\sim 10^{16}$ G in the stellar interior when ascribed to magnetic pressure.

As a first demonstration of the power of the *ASTRO-H* observation, we compared the νF_ν , *Suzaku* and *ASTRO-H* spectra of a bright anomalous X-ray pulsar 4U 0142+61 in Figure 20. Although the HXC was detected by *Suzaku* (Enoto et al., 2011), its spectral information is still poor above 80 keV (see Figure 20 left). On the other hand, as shown in Figure 20 right, *ASTRO-H* will detect the HXC up to 400 keV with 3σ level, when assuming 100 ksec exposure. In order to further estimate detectability of the cutoff, we compare the models with and without an exponential cut-off, indicating that *ASTRO-H* achieves the detection of the cut-off feature. Another bright magnetar, SGR 1806–20, was also simulated in Figure 22 (left). To obtain the same statistical significance, the required 50 ksec observation by *Suzaku* is reduced only to 30 ksec by *ASTRO-H*. Although the *Suzaku*/HXD and *INTEGRAL* has already detected the HXC up to ~ 20 keV (Esposito et al., 2007; Nakagawa et al., 2009; Enoto et al., 2010), *ASTRO-H* can extend it up to 100 keV, presumably providing a precise measurement of the HXC and confirming the proposed correlation by *Suzaku*. In Section 3.1, we also show the HXI+SGD simulation of the bright AXP 1E 1841–045, located in the SNR Kes 73, to illustrate the ability of *ASTRO-H* to pin down the nature of its hard X-ray emission (e.g in the light of magnetar versus fossil disk accretion models; see Figure 14, right).

ASTRO-H has the advantage over *NuSTAR* in that it will allow a *simultaneous* broadband coverage needed

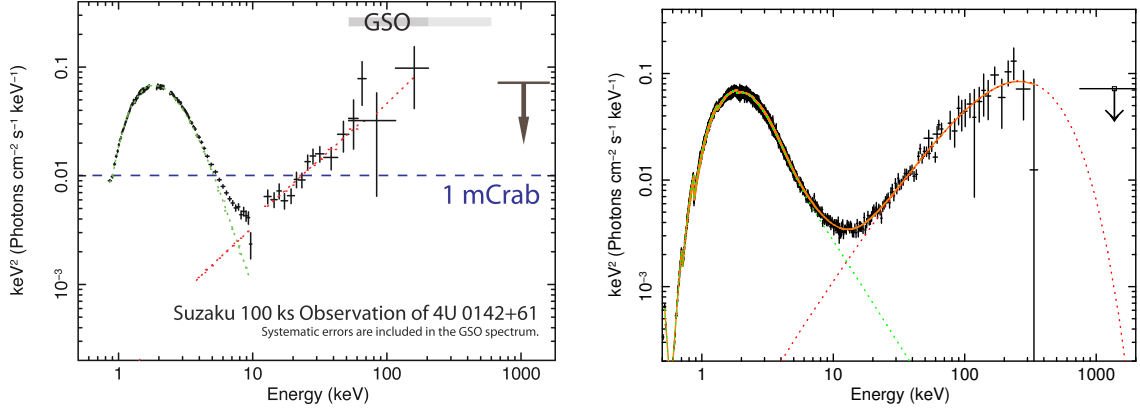


Figure 20: (Left) The 4U 0142+61 νF_ν spectrum obtained from the *Suzaku* 100 ksec observation (Enoto et al., 2011). (Right) Simulated 100 ks *ASTRO-H* 4U 0142+61 observation using the parameters of the *Suzaku* result. The HXC is reproduced by a single PL of $\Gamma_h = 0.11$ and the flux F_h of $29.7 \times 10^{-12} \text{ erg s}^{-1} \text{ cm}^{-2}$ in the 1-60 keV. The exponential cutoff is further added at 150 keV to satisfy the COMPTEL upper limit. Orange, dotted green, and red lines denote the best-fit model, SXC model and HXC model, respectively. The 2σ *CGRO*/COMPTEL upper-limits (Kuiper et al., 2006) are also plotted.

to study the SXC and HXC together (see also the potential for studying these sources with the Soft Gamma-ray Detector on board *ASTRO-H*, §3.4)

Contrary to the above three examples, the HXC from a famous anomalous X-ray pulsar, 1E2259+586 located in the SNR CTB 109 (see Section 3.1), has not yet been detected despite intensive observations with *INTEGRAL*, *RXTE* and *Suzaku*. (Kuiper et al., 2006; Enoto et al., 2011). If the correlation proposed by *Suzaku* is true, 1E 2259+586 may emit the HXC at $F_h = 3.9 \times 10^{-12} \text{ erg s}^{-1} \text{ cm}^{-2}$ based on the confirmed SXC $F_s = 7.3 \times 10^{-11} \text{ erg s}^{-1} \text{ cm}^{-2}$ with its characteristic age, 230 kyr. Here we employed an absorbed blackbody plus a power-law for the SXC and another hard power-law for the HXC. If there is no spectral break in the HXC and its photon index is between -1 and 1, *ASTRO-H*/HXI will clearly detect the HXC at least up to 50 keV with ~ 120 ks exposure time. On the other hand, without the spectral break, the HXC exceeded the the upper limits from COMPTEL (together with *Suzaku* and *INTEGRAL*), as seen in 4U 0141+61. Figure 22 (right) shows νF_ν spectrum when adding an exponential cut-off feature at 150 keV, together with upper-limits obtained from previous observations (Enoto et al., 2010; Kuiper et al., 2006). Even in this case, *ASTRO-H* will detect the HXC with a certain significance level, if the photon index is roughly 0, which is consistent with the correlation by *Suzaku*. Since 1E 2259+586 has the oldest characteristic age among magnetars observed with *Suzaku*, revealing the HXC spectrum of the object means to test whether the relation is applicable for all magnetars or not.

We finally evaluated detectability of the HXC from dim sources in 10-100 keV range. Figure 21 shows required exposure time to detect the HXC with a 3σ significance. Five magnetars indicated in the figure were observed with several X-ray observatories, but their weak HXC has not yet been reported so far. Assuming hard X-ray fluxes calculated by the broadband spectral correlation suggested by *Suzaku*, *ASTRO-H* will catch the HXC with a realistic exposure time (i.e., ~ 100 ksec). It should be also noted that the imaging capability of the HXI enables us to extract the hard X-ray spectrum from objects previously contaminated from nearby sources, e.g., CXO J164710.2–455216. Such a systematic study by *ASTRO-H* will help us reach a unified hard X-ray nature for this class.

3.4 How the burst activity is related with the nature of magnetars?

One of the prominent magnetar features are sporadic X-ray outbursts (flares) accompanied by short bursts which both are thought to be directly related to the magnetic energy release. However, the persistent HXC and short bursts during X-ray outbursts are poorly understood.

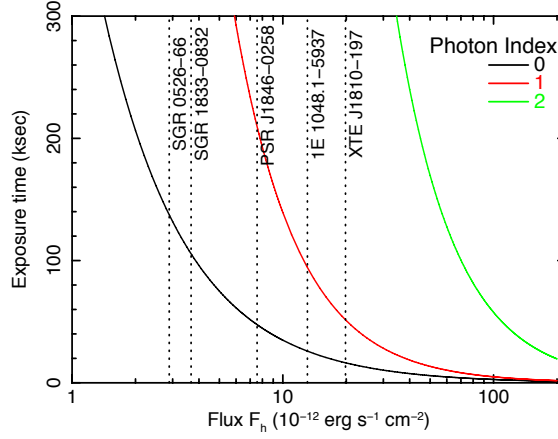


Figure 21: The HXC detectability with the HXI and SGD. Required exposure for HXC 3σ detections is plotted as a function of the 10–100 keV flux F_h , assuming a single PL with $\Gamma_h = 2$ (green), 1 (red), and 0 (black) and 3% systematic uncertainty of the non X-ray background. Dotted lines indicate assumed F_h of 5 magnetars assuming the correlation suggested by *Suzaku* (Enoto et al., 2010).

3.4.1 Unresolved spectral change during the X-ray outburst

The persistent SXC of magnetars sometimes increases during the outburst by one to two orders of magnitude with unpredictable timing. Such a transient enhancement lasts typically for a few months, with gradual decay. Figure 23a shows two recent sudden X-ray activations of the AXP 1E 1547.0-5408. As shown in Figure 23b, it is often accompanied, in its early phase, by short burst activities. These burst-active states have been already observed from some magnetars; XTE J1810–197 (Gotthelf et al., 2004), CXOU J164710.2–455216 (Israel et al., 2007), SGR 0501+4516 (Enoto et al., 2009), and 1E 1547.0-5408 (Mereghetti et al., 2009). More recently, there has been an increasing number of reports from magnetars with much weaker dipole fields ($\lesssim 4.4 \times 10^{13}$ G): SGR 0418+5729 (Rea et al., 2010), SGR 1833-0832 (Göğüş et al., 2010), Swift J1822.3-1606 (Rea et al., 2012), and Swift J1834.9–0846 (Kargaltsev et al., 2012). Figure 24a presents recent examples of the SXC flux decay of magnetars.

During the SXC outburst, an enhanced HXC above 10 keV has also been reported (Rea et al., 2009; Enoto et al., 2010d,c; Kuiper et al., 2012). While the SXC has been monitored in detail by *RXTE* and *Swift* during the decay phase, the HXC detections are still quite rare: only a few observations by *INTEGRAL* and *Suzaku* from SGR 0501+4516 in 2008 and 1E 1547.0-5408 in 2009. Actual spectra recorded by *Suzaku* are shown in Figure 24b and c, where the HXC was successfully detected with a flux of 2.7×10^{-11} erg s $^{-1}$ cm $^{-2}$ and 1.1×10^{-10} erg s $^{-1}$ cm $^{-2}$ in the 15–50 keV. However, they are just snapshots during the decay phase, and it is not yet clear how the HXC evolves during the outburst state and how the HXC is physically related with the SXC. Thus, the broadband spectral coverage for the SXC and HXC is expected to help resolve the emission mechanism and the postulated dissipation process of the magnetic energy.

Previous *Suzaku* ToOs (Figure 24) of 1E 1547.0–5408 and SGR 0501+4516 were performed ~ 4 and ~ 7 days after the onset of outburst, respectively. The HXC quickly decays to ~ 0.1 mCrab or less below the *Suzaku* detection limit within a few weeks. To compare *Suzaku* and *ASTRO-H*, we simulated, in Figure 25, the HXC monitoring of the X-ray outburst. While *Suzaku* HXD-PIN can not detect the HXC when ~ 3 weeks have passed after the onset of the outburst, *ASTRO-H* HXI still provides sufficient counts to detect the HXC within nearly a few “years” after the onset. These provide us, for the first time, with a detailed measurement of the HXC spectral evolution during the decay phase of magnetars.

So far, 2–3 magnetar outbursts have been detected per year. Recent accumulated discoveries of weak-field magnetars further suggest that there is a large hidden population of this kind of sources. The above continuous monitoring into the HXC provides us a way to investigate the connection between the quiescent and activated magnetars, which is vital to understand the evolutionary path of the magnetar class. The prompt one or two

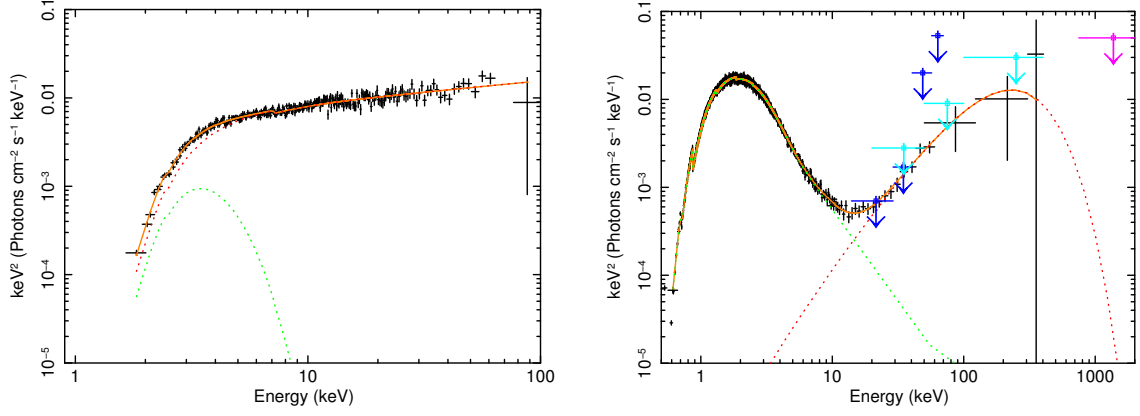


Figure 22: (Left) Expected νF_ν form of SGR 1806–20 observed by *ASTRO-H*. An absorbed blackbody plus a PL model is employed as a best-fit model based on the *Suzaku* observation. The orange, green dotted and red dotted curves are the total best fit model, SX and HXC, respectively. An absorbed blackbody plus a power-law model was employed. (Right) Same as left panel but for 1E 2259+586. The upper-limits are shown from *Suzaku* (blue, Enoto et al., 2010), *INTEGRAL* (light blue, Kuiper et al., 2006) and *CGRO* (magenta). [After compiling this white paper, the NuSTAR reported the hard X-rays (Vogel et al., 2014)]

ToO observations can provide us the physical conditions at an activated state, while the follow-up observations at once or twice per year during subsequent two years can further give us the decay trend of the hard X-rays (e.g., photon index, decay speed), e.g., Swift J1822.3-1606 (Rea et al., 2012), Swift J1834.90846 (Kargaltsev et al., 2012), and 3XMM J185246.6+003317 (Zhou et al., 2014; Rea et al., 2014).

3.4.2 Magnetar signatures in the short bursts and giant flares

One characteristic form of magnetar X-ray radiation is sporadic emission of bursts with a typical duration from ~ 0.1 second to a few hundred seconds. The burst mechanisms is thought to be related to the rearrangement of the B -field due to reconnections or motions of the NS crust (e.g., star quake). These bursts are phenomenologically classified into three types: “giant flares” ($L_x > 10^{45}$ erg s $^{-1}$, lasting about a few hundred seconds), “intermediate flares” ($L_x \sim 10^{42} - 10^{43}$ erg s $^{-1}$, lasting a few seconds), and frequently occurring “short bursts” ($L_x \sim 10^{38} - 10^{41}$ erg s $^{-1}$, ~ 0.1 -sec durations). These explosive events often show luminosities exceeding the Eddington limit for a NS of $1.4M_\odot$, $L_{\text{Edd}} \sim 1.8 \times 10^{38}$ erg s $^{-1}$, presumably due to suppression of the electron scattering cross sections in the strong B -field. These short bursts are thus attractive targets during the ToO observations.

Polarization of bursts: High polarization degree is expected from magnetars due to the high B -field. We simulated the polarization detectability of short bursts with SGD using a simulator provided by the SGD hardware team. We assumed short bursts from SGR 1806–20 ($N_H = 6 \times 10^{22}$ cm $^{-2}$, distance = 15 kpc) with spectral parameters of two-blackbody model ((Nakagawa et al., 2007): $R_{\text{HT}}^2/R_{\text{LT}}^2 = 0.01$, $kT_{\text{LT}} = 4$ keV, $kT_{\text{HT}} = 11$ keV). Figure 27 shows the expected polarization in different intensities when burst events accumulated. The burst rate of SGR 1806–20 in the active state was ~ 2 bursts/day observed by HETE-2 (Nakagawa et al., 2007). In this simulation, we can detect the polarization of bursts from SGR/AXP when we observe bright bursts in the active state.

Proton CRSF: Proton CRSF is a potential interesting target of the short burst using the *ASTRO-H* SXS as already discussed in §3.1.

Is the persistent emission composed of unresolved short bursts? The enhanced persistent and burst emissions have been simultaneously observed in many activated magnetars. However, it is not yet clear how these two emission forms are physically related to each other. One interesting possibility is that the persistent emission is composed of a large number of small bursts that are not individually detectable. Such a possibility has been examined using a cumulative number-intensity distribution of short bursts. The observational information has so far remained insufficient to evaluate this possibility, since the studied short bursts are so bright (with

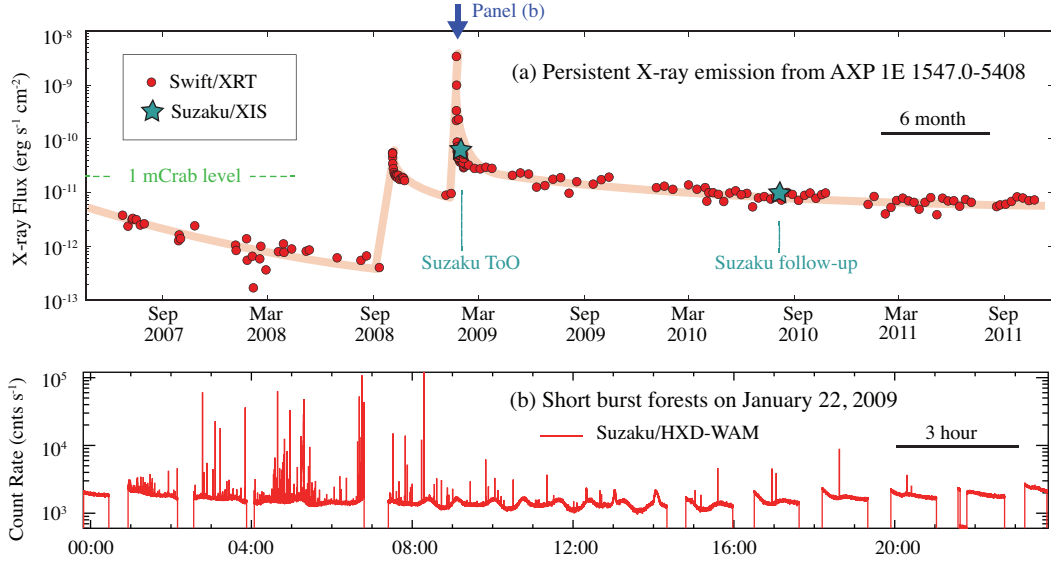


Figure 23: (a) A long-term SXC monitoring of AXP 1E 1547.0–5408 with *Swift*/XRT, with the absorbed 2–10 keV X-ray flux shown. Two *Suzaku* observations are also shown in green stars (Enoto et al., 2010c). (b) Short burst forests from this source recorded by *Suzaku*/HXD-WAM on January 22, 2009, indicated by a blue arrow in panel (a).

fluence $> 10^{-7}$ ergs cm $^{-2}$) and infrequent that their time-averaged flux is much lower than that of the persistent emission. It is interesting to examine, from observations of activated magnetars, whether weaker short bursts become similar in spectral shape to the persistent X-ray emission, as recently found in SGR 0501+4516 (Nakagawa et al., 2011). The high sensitivity of *ASTRO-H* can provide further studies connecting the persistent to burst emissions.

Advantages of the SGD shield detector: So far there is no clear detection of MeV photons from magnetar bursts except for during giant flares. MeV photons of magnetar bursts are an important key to investigate the radiation mechanism and physics in the strong B -field because photon splitting effect may suppress the high energy photons. In order to explore the MeV photons from short bursts, more photon statistics with fine time resolution is essentially needed. The *Suzaku* Wide-band All-sky Monitor (WAM) has reported a hint of MeV photons from one strong short burst from AXP 1E1547–5408 (Yasuda et al., in prep), but the lack of time resolution prevented a detailed investigation. The Soft Gamma-ray Detector (SGD) onboard *ASTRO-H* is surrounded by large Bi $_4$ Ge $_3$ O $_{12}$ crystals to reduce the cosmic and gamma-ray backgrounds (Figure 26). This active shield with a wide field-of-view is available as an all-sky monitor covering ~ 200 keV to 5 MeV. The most notable features are a large effective area (~ 800 cm 2 even at 1 MeV) roughly twice to the *Suzaku* WAM, fine time resolution (16 ms), and fine spectral resolution (32 channel than 4 channel of the *Suzaku* WAM). The *Suzaku* WAM has to disable triggers until the onboard triggered data is transferred to the spacecraft memory at the next SAA passage, while the SGD active shield can minimize this latency and the triggered data is immediately transferred. These features become a powerful tool to study magnetar short burst especially with large photon statistics and fine time resolution.

Figure 28 shows a simulated spectrum of the intense short burst from AXP 1E1547–5408, which has a signature of MeV photons³. The SGD monitor can clearly detect up to 2 MeV, and distinguish different spectral models, such as 2BB and BB+PL. Figure 27 shows the observable flux range of SGD shield detectors. We can expect that bright short bursts and intermediate flares are good targets for SGD shield detectors.

³Due to readout deadtime and counter rollover effect, the data from the SGD shield detectors should be subject to some corrections such as pile-up or carry over of observed counts. The estimated maximum brightness of bursts which free from such corrections is about 100 Crab, and 1000 Crab would be also observable with some corrections. From spectral simulations, a possible detection limit is found to be about 1 Crab.

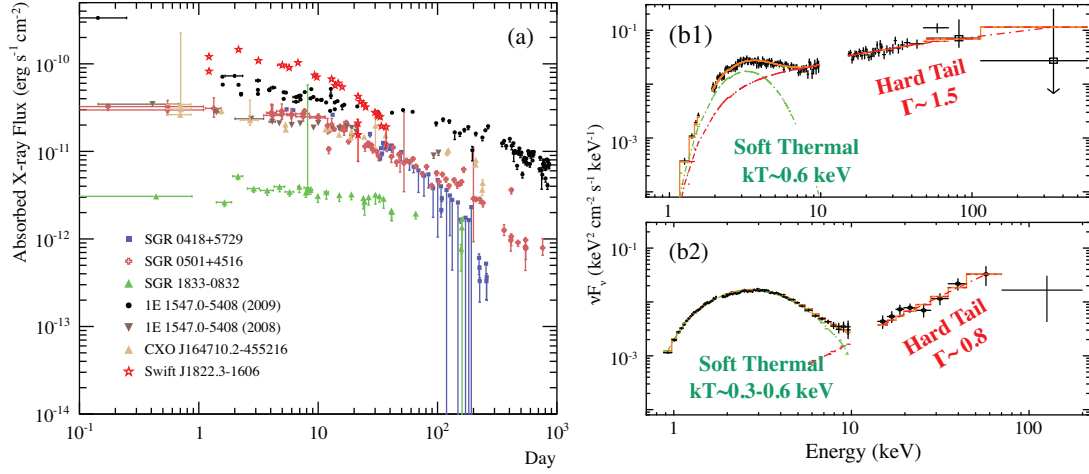


Figure 24: (a) Absorbed 2–10 keV X-ray fluxes of transient magnetars monitored with *Swift*/XRT, *RXTE*/PCA, and *Suzaku*/XIS. The time onset corresponds to the first detection of magnetar short bursts from these sources, mainly detected with *Swift*/BAT. (b) *Suzaku* spectra during recent two transient activities of 1E 1547.0–5408 (b1) and SGR 0501+4516 (b2) (Enoto et al., 2010c,d).

Acknowledgements

We thank Matthias Kühnel (Remeis Observatory & FAU, Germany) for substantial contributions to preparing Figures 3 and 8 as well as for valuable comments on an earlier version of the manuscript.

4 Appendix

4.1 Acronym

AXP

Anomalous X-ray Pulsar.

BAT

Burst Alert Telescope onboard *Swift*.

CCD

Charge Coupled Device.

CCO

Central Compact Object.

CRSF

Cyclotron Resonance Scattering Feature.

CSM

Circumstellar Medium.

GRLB

Gamma-ray Loud Binary.

HMXB

High Mass X-ray Binary.

HXC

Hard X-ray Component of magnetar X-ray spectra (>10 keV).

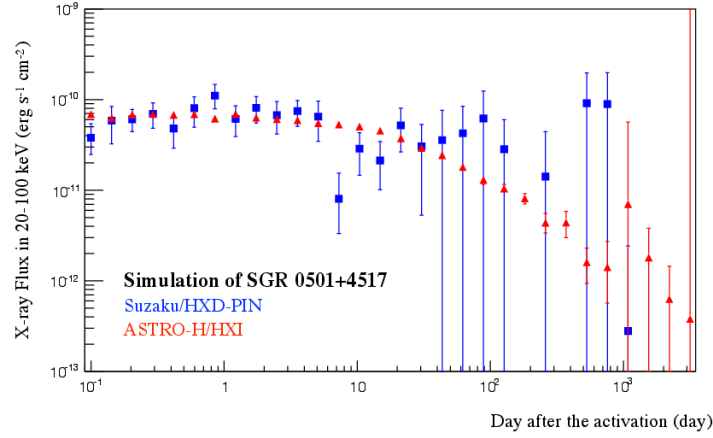


Figure 25: Simulations of the HXC monitoring toward an activated SGR 0501+4516 in 2008. The spectral shape is assumed to be the same as that observed by *Suzaku* in 2008, and normalized to have the same decaying speed as the SXC. Blue and Red data points are simulated X-ray fluxes in the 20–100 keV measured by *Suzaku*/HXD-PIN and *ASTRO-H*/HXI, respectively. Both exposures are set to be 40 ksec (90% confidence level errors).

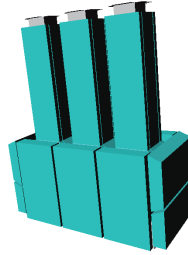


Figure 26: A schematic picture of Soft Gamma-ray Detector (SGD). The main detector of SGD is surrounded by large and thick 25 BGO crystals.

HXD

Hard X-ray Detector onboard *Suzaku*.

HXI

Hard X-ray Imager onboard *ASTRO-H*.

ISM

Interstellar Medium. .

LMXB

Low Mass X-ray Binary.

LPP

Long Period Pulsar.

NS

Neutron Star.

PCA

Proportional Counter Array onboard *RXTE*.

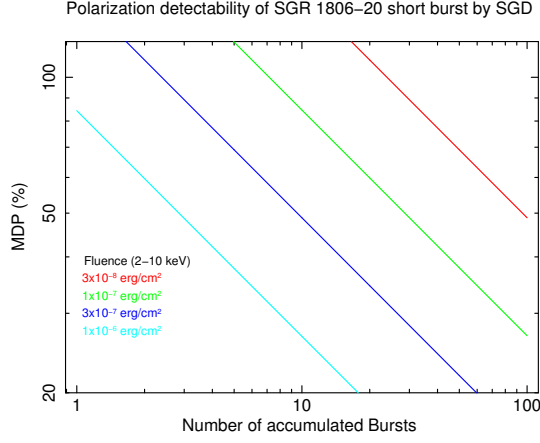


Figure 27: Simulated polarization detectability from accumulated short burst events by SGD. Spectrum from 1806-20 bursts were assuming two black body model: $\frac{R_{\text{HT}}}{R_{\text{LT}}}^2 = 0.01$, $kT_{\text{LT}} = 4$ keV, $kT_{\text{HT}} = 11$ keV (Nakagawa et al., 2007) in varied burst intensities.

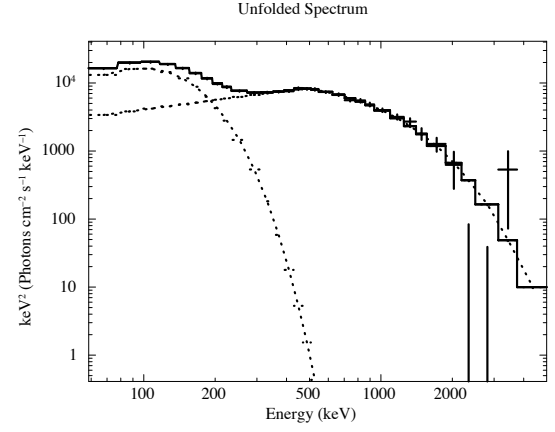


Figure 28: Spectral simulation of one of the bright bursts of AXP 1E1547-5408 with the SGD shield detectors. Assumed spectral model is blackbody plus power-law model as reported in Yasuda et al. (in prep). Dashed-lines shows each spectral model component and the solid line represents the total model.

QED

Quantum Electrodynamics.

RPP

Rotation Powered Pulsar.

RRAT

Rotating Radio Transient.

RXTE

Rossi X-ray Timing Explorer.

SCF-effect

Self Charge Filling effect.

SFXT

Supergiant Fast X-ray Transient.

SGD

Soft Gamma-ray Detector onboard *ASTRO-H*.

SGR

Soft Gamma Repeater.

SNR

Supernova Remnant.

SXC

Soft X-ray Component of magnetar X-ray spectra (<10 keV).

SXI

Soft X-ray Imager onboard *ASTRO-H*.

SXS

Soft X-ray Spectrometer onboard *ASTRO-H*.

ToO

Target of Opportunity.

VHE γ -ray

Vert High Energy γ -ray.

WAM

Wide-band All-sky Monitor onboard *Suzaku*.

XDINS

X-ray Dim Isolated Neutron Star.

XIS

X-ray Imaging Spectrometer onboard *Suzaku*.

XRBP

X-ray Binary Pulsar.

References

- Abdo, A. A., Ackermann, M., Ajello, M., et al. 2010, *ApJ*, 725, L73
- Aharonian, F., Akhperjanian, A. G., Aye, K.-M., et al. 2005, *A&A*, 442, 1
- Aharonian, F., Akhperjanian, A. G., Bazer-Bachi, A. R., et al. 2006a, *A&A*, 460, 743
- . 2006b, *ApJ*, 636, 777
- Albert, J., Aliu, E., Anderhub, H., et al. 2006, *Science*, 312, 1771
- Alpar, M. A., Ankay, A., & Yazgan, E. 2001, *ApJ*, 557, L61
- An, H., Hascoët, R., Kaspi, V. M., et al. 2013a, *ApJ*, 779, 163
- Araya-Góchez, R. A., & Harding, A. K. 2000, *ApJ*, 544, 1067
- Baring, M. G., & Harding, A. K. 2007, *Ap&SS*, 308, 109
- Basko, M. M., & Sunyaev, R. A. 1976, *MNRAS*, 175, 395
- Becker, P. A., Klochkov, D., Schönherr, G., et al. 2012, *A&A*, 544, A123
- Bednarek, W. 2009, *MNRAS*, 397, 1420
- Beloborodov, A. M. 2013, *ApJ*, 777, 114
- Bodaghee, A., Tomsick, J. A., Rodriguez, J., et al. 2011, *ApJ*, 727, 59
- Boella, G., Butler, R. C., Perola, G. C., et al. 1997, *A&AS*, 122, 299
- Bozzo, E., Falanga, M., & Stella, L. 2008, *ApJ*, 683, 1031
- Bozzo, E., Giunta, A., Cusumano, G., et al. 2011, *A&A*, 531, A130
- Bradt, H. V., Rothschild, R. E., & Swank, J. H. 1993, *A&AS*, 97, 355
- Brandt, W. N., & Schulz, N. S. 2000, *ApJ*, 544, L123
- Caballero, I., & Wilms, J. 2012, *Mem. Soc. Astron. Italiana*, 83, 230
- Chernyakova, M., Neronov, A., Aharonian, F., Uchiyama, Y., & Takahashi, T. 2009, *MNRAS*, 397, 2123
- Colpi, M., Geppert, U., & Page, D. 2000, *ApJ*, 529, L29
- Davidson, K., & Ostriker, J. P. 1973, *ApJ*, 179, 585
- Doroshenko, V., Santangelo, A., Suleimanov, V., et al. 2010, *A&A*, 515, A10
- Duncan, R. C., & Thompson, C. 1992, *ApJ*, 392, L9
- Duncan, R. C., & Thompson, C. 1996, in *American Institute of Physics Conference Series*, Vol. 366, *High Velocity Neutron Stars*, ed. R. E. Rothschild & R. E. Lingelfelter, 111–117
- Enoto, T., Makishima, K., Nakazawa, K., et al. 2011, *PASJ*, 63, 387
- Enoto, T., Nakazawa, K., Makishima, K., et al. 2010a, *ApJ*, 722, L162
- Enoto, T., Nakagawa, Y. E., Rea, N., et al. 2009, *ApJ*, 693, L122
- Enoto, T., Nakazawa, K., Makishima, K., et al. 2010c, *PASJ*, 62, 475
- Enoto, T., Rea, N., Nakagawa, Y. E., et al. 2010d, *ApJ*, 715, 665
- Ertan, Ü., Ekşi, K. Y., Erkut, M. H., & Alpar, M. A. 2009, *ApJ*, 702, 1309
- Esposito, P., Mereghetti, S., Tiengo, A., et al. 2007, *A&A*, 476, 321
- Feldmeier, A., Rätzel, D., & Owocki, S. P. 2008, *ApJ*, 679, 704
- Ferrand, G., & Safi-Harb, S. 2012, *Advances in Space Research*, 49, 1313
- Frank, J., King, A., & Raine, D. J. 2002, *Accretion Power in Astrophysics*, ISBN: 0521620538
- Fürst, F., Kreykenbohm, I., Pottschmidt, K., et al. 2010, *A&A*, 519, A37
- Fürst, F., Suchy, S., Kreykenbohm, I., et al. 2011, *A&A*, 535, A9
- Gaensler, B. M., McClure-Griffiths, N. M., Oey, M. S., et al. 2005, *ApJ*, 620, L95
- Gavriil, F. P., Dib, R., & Kaspi, V. M. 2008a, in *American Institute of Physics Conference Series*, Vol. 983, *40 Years of Pulsars: Millisecond Pulsars, Magnetars and More*, ed. C. Bassa, Z. Wang, A. Cumming, & V. M. Kaspi, 234–238
- Gavriil, F. P., Dib, R., & Kaspi, V. M. 2008b, in *American Institute of Physics Conference Series*, Vol. 983, *40 Years of Pulsars: Millisecond Pulsars, Magnetars and More*, ed. C. Bassa, Z. Wang, A. Cumming, & V. M. Kaspi, 234–238
- Gavriil, F. P., Gonzalez, M. E., Gotthelf, E. V., et al. 2008c, *Science*, 319, 1802
- Gavriil, F. P., Kaspi, V. M., & Woods, P. M. 2002, *Nature*, 419, 142
- . 2006, *ApJ*, 641, 418
- Gotthelf, E. V., & Halpern, J. P. 2009, *ApJ*, 695, L35
- Gotthelf, E. V., Halpern, J. P., & Alford, J. 2013, *ApJ*, 765, 58
- Gotthelf, E. V., Halpern, J. P., Buxton, M., & Bailyn, C. 2004, *ApJ*, 605, 368
- Göğüş, E., Cusumano, G., Levan, A. J., et al. 2010, *ApJ*, 718, 331
- Grebenev, S. A., & Sunyaev, R. A. 2007, *Astronomy Letters*, 33, 149
- Grefenstette, B. W., Harrison, F. A., Boggs, S. E., et al. 2014, *Nature*, 506, 339
- Hanke, M., Wilms, J., Nowak, M. A., et al. 2009a, *ApJ*, 690, 330
- Hanke, M., Wilms, J., Nowak, M. A., et al. 2009b, in *Chandra's First Decade of Discovery*, ed. S. Wolk, A. Fruscione, & D. Swartz

- Harding, A. K., & Lai, D. 2006, *Reports on Progress in Physics*, 69, 2631
- Harrison, F. A., Craig, W. W., Christensen, F. E., et al. 2013, *ApJ*, 770, 103
- Ho, W. C. G., & Heinke, C. O. 2009, *Nature*, 462, 71
- Ho, W. C. G., & Lai, D. 2001, *MNRAS*, 327, 1081
- Iaria, R., Di Salvo, T., Robba, N. R., et al. 2005, *ApJ*, 634, L161
- Ibrahim, A. I., Safi-Harb, S., Swank, J. H., et al. 2002, *ApJ*, 574, L51
- Ibrahim, A. I., Swank, J. H., & Parke, W. 2003, *ApJ*, 584, L17
- Ibrahim, A. I., Markwardt, C. B., Swank, J. H., et al. 2004, *ApJ*, 609, L21
- in't Zand, J. J. M. 2005, *A&A*, 441, L1
- Isenberg, M., Lamb, D. Q., & Wang, J. C. L. 1998, *ApJ*, 505, 688
- Israel, G. L., Campana, S., Dall'Osso, S., et al. 2007, *ApJ*, 664, 448
- Iwahashi, T., Enoto, T., Yamada, S., et al. 2013, *PASJ*
- Iwasawa, K., Koyama, K., & Halpern, J. P. 1992a, *PASJ*, 44, 9
- Johnston, S., Ball, L., Wang, N., & Manchester, R. N. 2005, *MNRAS*, 358, 1069
- Kargaltsev, O., Kouveliotou, C., Pavlov, G. G., et al. 2012, *ApJ*, 748, 26
- Kaspi, V. M. 2010, ArXiv e-prints, arXiv:1005.0876
- Klochkov, D., Santangelo, A., Staubert, R., & Ferrigno, C. 2008, *A&A*, 491, 833
- Klochkov, D., Staubert, R., Santangelo, A., Rothschild, R. E., & Ferrigno, C. 2011, *A&A*, 532, A126+
- Klochkov, D., Horns, D., Santangelo, A., et al. 2007, *A&A*, 464, L45
- Klochkov, D., Doroshenko, V., Santangelo, A., et al. 2012, *A&A*, 542, L28
- Koljonen, K. I. I., McCollough, M. L., Hannikainen, D. C., & Droulans, R. 2013, *MNRAS*, 429, 1173
- Kreykenbohm, I., Coburn, W., Wilms, J., et al. 2002, *A&A*, 395, 129
- Kreykenbohm, I., Wilms, J., Kretschmar, P., et al. 2008, *A&A*, 492, 511
- Kuehnel, M., Mueller, S., Kreykenbohm, I., et al. 2012, *The Astronomer's Telegram*, 4564, 1
- Kuiper, L., Hermsen, W., den Hartog, P. R., & Collmar, W. 2006, *ApJ*, 645, 556
- Kuiper, L., Hermsen, W., den Hartog, P. R., & Urama, J. O. 2012, *ApJ*, 748, 133
- Kumar, H. S., & Safi-Harb, S. 2008, *ApJ*, 678, L43
- Kumar, H. S., Safi-Harb, S., & Gonzalez, M. E. 2012, *ApJ*, 754, 96
- Kumar, H. S., Safi-Harb, S., Slane, P. O., & Gotthelf, E. V. 2014, *ApJ*, 781, 41
- Kylafis, N. D., Trümper, J. E., & Ertan, Ü. 2014, *A&A*, 562, A62
- La Barbera, A., Santangelo, A., Orlandini, M., & Segreto, A. 2003, *A&A*, 400, 993
- Lai, D., & Ho, W. C. G. 2002, *ApJ*, 566, 373
- Lattimer, J. M., & Prakash, M. 2007, *Phys. Rep.*, 442, 109
- Li, J., Torres, D. F., Zhang, S., et al. 2011, *ApJ*, 733, 89
- Maitra, C., & Paul, B. 2013, *ApJ*, 763, 79
- Makishima, K., Enoto, T., Hiraga, J. S., et al. 2014, *Physical Review Letters*, 112, 171102
- Makishima, K., Mihara, T., Nagase, F., & Tanaka, Y. 1999, *ApJ*, 525, 978
- Makishima, K., Ohashi, T., Sakao, T., et al. 1988, *Nature*, 333, 746
- Malheiro, M., Rueda, J. A., & Ruffini, R. 2012, *PASJ*, 64, 56
- Malygin, M. G., & Iakubovskiy, D. A. 2011, in *Young Scientists 17th Proceedings*, ed. V. Editors: Choliy, G. Ivashchenko, & O. Ivaniuk, 43–46
- Manchester, R. N., Hobbs, G. B., Teoh, A., & Hobbs, M. 2005, *AJ*, 129, 1993
- Manousakis, A., Walter, R., & Blondin, J. M. 2012a, *A&A*, 547, A20
- . 2012b, *A&A*, 547, A20
- Mereghetti, S. 2008, *A&A Rev.*, 15, 225
- Mereghetti, S., Götz, D., Weidenspointner, G., et al. 2009, *ApJ*, 696, L74
- Meszaros, P., Novick, R., Szentgyorgyi, A., Chanan, G. A., & Weisskopf, M. C. 1988, *ApJ*, 324, 1056
- Mitsuda, K., Bautz, M., Inoue, H., et al. 2007, *Publications of the Astronomical Society of Japan*, 59, 1
- Morton, T. D., Slane, P., Borkowski, K. J., et al. 2007, *ApJ*, 667, 219
- Nagase, F., Corbet, R. H. D., Day, C. S. R., et al. 1992, *ApJ*, 396, 147
- Naik, S., Paul, B., & Ali, Z. 2011, *ApJ*, 737, 79
- Nakagawa, Y. E., Makishima, K., & Enoto, T. 2011a, *PASJ*, 63, 813
- Nakagawa, Y. E., Yoshida, A., Hurley, K., et al. 2007a, *PASJ*, 59, 653

- Nakagawa, Y. E., Mihara, T., Yoshida, A., et al. 2009, *PASJ*, 61, 387
- Negueruela, I., Okazaki, A. T., Fabregat, J., et al. 2001, *A&A*, 369, 117
- Negueruela, I., & Smith, D. M. 2006, The Astronomer's Telegram, 831, 1
- Nomoto, K., Tominaga, N., Umeda, H., Kobayashi, C., & Maeda, K. 2006, *Nuclear Physics A*, 777, 424
- Olive, J.-F., Hurley, K., Sakamoto, T., et al. 2004, *ApJ*, 616, 1148
- Oosterbroek, T., Parmar, A. N., Rea, N., et al. 2004, in *ESA Special Publication*, Vol. 552, 5th *INTEGRAL* Workshop on the *INTEGRAL* Universe, ed. V. Schoenfelder, G. Lichti, & C. Winkler, 471
- Oskinova, L. M., Hamann, W.-R., & Feldmeier, A. 2007, *A&A*, 476, 1331
- Ouyed, R., Leahy, D., & Koning, N. 2014, ArXiv e-prints, arXiv:1404.5063
- Ouyed, R., Niebergal, B., Dobler, W., & Leahy, D. 2006, *ApJ*, 653, 558
- Owocki, S. P., & Cohen, D. H. 2001, *ApJ*, 559, 1108
- Özel, F. 2003, *ApJ*, 583, 402
- Paerels, F., Cottam, J., Sako, M., et al. 2000, *ApJ*, 533, L135
- Pringle, J. E., & Rees, M. J. 1972, *A&A*, 21, 1
- Rampy, R. A., Smith, D. M., & Negueruela, I. 2009, *ApJ*, 707, 243
- Rea, N., Israel, G. L., & Stella, L. 2004a, *Nuclear Physics B Proceedings Supplements*, 132, 554
- Rea, N., Israel, G. L., Stella, L., et al. 2003a, *ApJ*, 586, L65
- Rea, N., Israel, G. L., Oosterbroek, T., et al. 2007, *Ap&SS*, 308, 505
- Rea, N., Israel, G. L., Turolla, R., et al. 2009, *MNRAS*, 396, 2419
- Rea, N., Esposito, P., Turolla, R., et al. 2010, *Science*, 330, 944
- Rea, N., Israel, G. L., Esposito, P., et al. 2012, *ApJ*, 754, 27
- Rea, N., Viganò, D., Israel, G. L., Pons, J. A., & Torres, D. F. 2014, *ApJ*, 781, L17
- Reig, P. 2011, *Ap&SS*, 332, 1
- Romano, P., Krimm, H. A., Palmer, D. M., et al. 2014, *A&A*, 562, A2
- Safi-Harb, S. 2013, in *IAU Symposium*, Vol. 291, *IAU Symposium*, 251–256
- Safi-Harb, S., & Kumar, H. S. 2013, in *IAU Symposium*, Vol. 291, *IAU Symposium*, 480–482
- Sako, M., Kahn, S. M., Paerels, F., et al. 2002, in *High Resolution X-ray Spectroscopy with XMM-Newton and Chandra*, ed. G. Branduardi-Raymont
- Sasaki, M., Plucinsky, P. P., Gaetz, T. J., & Bocchino, F. 2013, *A&A*, 552, A45
- Sasaki, M., Plucinsky, P. P., Gaetz, T. J., et al. 2004, *ApJ*, 617, 322
- Schönherr, G., Wilms, J., Kretschmar, P., et al. 2007, *ApJ*, 472, 353
- Schulz, N. S., Canizares, C. R., Lee, J. C., & Sako, M. 2002, *ApJ*, 564, L21
- Sguera, V., Barlow, E. J., Bird, A. J., et al. 2005, *A&A*, 444, 221
- Smith, A., Kaaret, P., Holder, J., et al. 2009, *ApJ*, 693, 1621
- Smith, D. M., Negueruela, I., Heindl, W. A., Markwardt, C. B., & Swank, J. H. 2004, in *Bulletin of the American Astronomical Society*, Vol. 36, *AAS/High Energy Astrophysics Division* #8, 954
- Staubert, R., Klochkov, D., Postnov, K., et al. 2009, *A&A*, 494, 1025
- Strohmayer, T. E., & Ibrahim, A. I. 2000, *ApJ*, 537, L111
- Suchy, S., Fürst, F., Pottschmidt, K., et al. 2012, *ApJ*, 745, 124
- Suchy, S., Pottschmidt, K., Wilms, J., et al. 2008, *ApJ*, 675, 1487
- Szostek, A., Zdziarski, A. A., & McCollough, M. L. 2008, *MNRAS*, 388, 1001
- Taylor, J. H., & Weisberg, J. M. 1982, *ApJ*, 253, 908
- Thompson, C., & Beloborodov, A. M. 2005, *ApJ*, 634, 565
- Thompson, C., & Duncan, R. C. 1995, *MNRAS*, 275, 255
- Tiengo, A., Esposito, P., Mereghetti, S., et al. 2013, *Nature*, 500, 312
- Todoroki, S., Kitamoto, S., Yoshida, Y., & Murakami, H. 2012, *PASJ*, 64, 101
- Torres, D. F., Rea, N., Esposito, P., et al. 2012, *ApJ*, 744, 106
- Truemper, J., Pietsch, W., Reppin, C., et al. 1978, *ApJ*, 219, L105
- Tsygankov, S. S., Lutovinov, A. A., & Serber, A. V. 2010, *MNRAS*, 401, 1628
- Turter, C. B., Tucker, W., & Salpeter, E. E. 1969, *ApJ*
- Uchiyama, Y., Tanaka, T., Takahashi, T., Mori, K., & Nakazawa, K. 2009, *ApJ*, 698, 911
- Vink, J. 2008, *Advances in Space Research*, 41, 503
- Vink, J., & Kuiper, L. 2006, *MNRAS*, 370, L14
- Vogel, J. K., Hascoët, R., Kaspi, V. M., et al. 2014, *ApJ*, 789, 75
- Walter, R., & Zurita Heras, J. 2007, *A&A*, 476, 335
- Wang, N., Johnston, S., & Manchester, R. N. 2004, *MNRAS*, 351, 599

- Wasserman, I., & Shapiro, S. L. 1983, *ApJ*, 265, 1036
- Watanabe, S., Sako, M., Ishida, M., et al. 2003, *ApJ*, 597, L37
- Watanabe, S., Sako, M., Ishida, M., et al. 2006, arXiv.org, astro-ph, 421
- Wilson, C. A., Finger, M. H., & Camero-Arranz, A. 2008, *ApJ*, 678, 1263
- Wojdowski, P. S., Liedahl, D. A., Sako, M., Kahn, S. M., & Paerels, F. 2003, *ApJ*, 582, 959
- Woods, P. M., & Thompson, C. 2006, Soft gamma repeaters and anomalous X-ray pulsars: magnetar candidates (Cambridge University Press), 547–586
- Woods, P. M., Kouveliotou, C., Gavriil, F. P., et al. 2005, *ApJ*, 629, 985
- Woosley, S. E., & Weaver, T. A. 1995, *ApJS*, 101, 181
- Zane, S., Turolla, R., Stella, L., & Treves, A. 2001, *ApJ*, 560, 384
- Zdziarski, A. A., Neronov, A., & Chernyakova, M. 2010, *MNRAS*, 403, 1873
- Zhou, P., Chen, Y., Li, X.-D., et al. 2014, *ApJ*, 781, L16